PHYSICAL REVIEW C VOLUME 20, NUMBER 5 NOVEMBER 1979

^{20}Ne states observed via $^{16}O(\alpha,\alpha_i)^{16}O$

James H. Billen
University of Wisconsin, Madison, Wisconsin 53706
(Received 18 June 1979)

Surface barrier detectors at 16–18 angles measured simultaneously the differential cross sections for the reactions $^{16}O(\alpha,\alpha_0\alpha_1\alpha_2\alpha_3\alpha_4\alpha_5)^{16}O$ in the bombarding energy range from 14.6 to 20.4 MeV and in steps of 10 keV. For $E_\alpha > 18$ MeV peak fitting techniques separated the yields of α_1 ($Q = -6.05$ MeV) from α_2 ($Q = -6.13$ MeV). The target was a differentially pumped windowless gas target of high purity O_2. A total of 25 levels in ^{20}Ne ($16 < E_x < 21$ MeV) were analyzed by writing the reaction amplitude for spinless positive-parity particles as a nonresonant term which varies linearly with energy plus a sum over only resonant partial waves. Inelastic scattering angular distributions were expanded in terms of Legendre polynomials for $E_\alpha > 18$ MeV.

[NUCLEAR REACTIONS $^{16}O(\alpha,\alpha_0\alpha_1\alpha_2\alpha_3\alpha_4\alpha_5)^{16}O$, $14.6 \leq E_\alpha \leq 20.4$ MeV, $\Delta E_\alpha = 10$ keV; measured $\sigma(E,\theta)$ at 18 angles. Deduced ^{20}Ne level parameters J, π, Γ_{α_0}, Γ_{α_1}, Γ, E_R. O_2 gas target.]

I. INTRODUCTION

One of the important features of previous work on the scattering of alpha particles by ^{16}O has been the persistence of resonant behavior correlated at widely separated angles. Such behavior is characteristic of compound nucleus formation. Mehta, Hunt, and Davis[1] at Florida State University inferred the existence of 35 states in ^{20}Ne between 12.7 and 20 MeV of excitation from elastic scattering (α_0) excitation functions at eight laboratory angles. Bergman and Hobbie[2] at the University of Minnesota observed a similar structure up to 26-MeV excitation in the α_0 and in the inelastic scattering (α_{1+2}) excitation functions. More recently Häusser *et al.*[3] at Chalk River scanned the energy range between 16.0 and 18.4 MeV in ^{20}Ne with very fine resolution (3–4 keV) and observed several levels with $\Gamma_{c.m.} < 100$ keV. Unfortunately none of the previous studies employed detectors at more than eight laboratory angles and hence, relatively few of the spin-parity assignments for the observed ^{20}Ne levels are unambiguous. Furthermore, except for some unresolved α_{1+2} measurements[2,3] and the $E_\alpha = 18.3$-MeV angular distribution of Corelli *et al.*,[4] no one has reported inelastic scattering of α particles to individual low-lying ^{16}O states.

The present paper reports data on the elastic scattering of alpha particles by ^{16}O and on the inelastic scattering to the first five excited states of ^{16}O for the bombarding energy range from $E_\alpha = 14.6$ to 20.4 MeV in steps of 10 keV. For bombarding energies between 14.6 and 18 MeV the measurements consist of α_0, α_{1+2}, α_3, and α_4 excitation functions taken simultaneously at 16 angles and in E_α steps of 10 keV. For bombarding energies between 18 and 20.4 MeV we have α_0, α_1, α_2, α_3, α_4, and α_5 excitation functions at 21 different angles taken in two scans of the energy region. The first scan employed detectors at 18 angles and E_α steps of 10 keV while the second used detectors at five angles and 10–30-keV steps. Two of the detectors were at the same angles in both scans. The measured data points total nearly 52 000.

Our analysis of these data focuses on the $^{16}O(\alpha,\alpha_0)^{16}O$(g.s.) and on the $^{16}O(\alpha,\alpha_1)^{16}O$(6.05 MeV) reactions, both of which involve only spinless positive-parity (0^+) particles. To extract resonant energies and widths from both the α_0 and the α_1 data I wrote the scattering amplitude as a linearly energy dependent nonresonant term plus a sum over only resonant partial waves. Fourteen ^{20}Ne levels observed via elastic scattering and 11 observed via inelastic scattering were analyzed in this manner. In addition we performed Legendre polynomial expansions of the angular distributions for the other inelastic scattering cross sections in the energy range $E_\alpha = 18$ to 20.4 MeV. However, the spin systems for these reactions ($0^+ + 0^+ \rightarrow 0^+ + I^\pi$; $I^\pi = 3^-$, 2^+, 1^-, and 2^- for α_2, α_3, α_4, and α_5, respectively) complicate tremendously the interpretation of the Legendre expansions.

II. EXPERIMENTAL PROCEDURE

Detector arrays of up to 18 totally depleted surface barrier detectors measured simultaneously the angular distributions of elastically and inelastically scattered alpha particles. A target consisting of differentially pumped O_2 gas (99.995%

pure) was bombarded by the He^{++} beam from our Pelletron-charged EN tandem Van de Graaff. After standard electronic signal processing, each detector's spectra were stored in the memory of our DDP-124 computer where they could be monitored on line, written on magnetic tape, and later recalled for analysis.

The data span the range of incident α particle energies E_α from 14.6 to 20.4 MeV, but because of important differences in the experimental arrangements for E_α above and below 18.0 MeV we distinguish between data set 1 (DS-1) corresponding to beam energies from 14.6 to 18.0 MeV and data set 2 (DS-2) with beam energies from 18.0 to 20.4 MeV. The spectra of DS-1 were measured in steps of 10 keV with a gas target pressure of 11 Torr and with a sixteen-detector angular array. The higher energy region was scanned twice, both times with a gas target pressure of 4 Torr. One scan covered the energy range from 18.0 to 20.4 MeV in steps of 10 keV with an eighteen-detector angular array, while another scan covered the same energy range in steps of 10–30 keV with a five-detector array optimized for forward angle detectors.

Spectral resolution was much better for DS-2 than for DS-1. The collimating slit systems used for DS-1 had an average angular acceptance of approximately 1.9° which, combined with the gas pressure of 11 Torr, corresponds to target thicknesses viewed by the detectors of 2–10 keV (largest at extreme forward and backward angles). Differential energy loss and energy straggling along the target-to-detector path (of 12.7 cm) broadened considerably the α peaks in the DS-1 spectra. Groups corresponding to inelastically scattered alphas (which have >6 MeV less energy than alpha particles elastically scattered by ^{16}O) were most affected. For DS-2 we used new collimating slit systems (average angular acceptance of 1.3°) and lower gas pressures to reduce the peak broadening caused by these kinematic effects. The higher bombarding energy for DS-2 also helped since the energy loss $-dE/dx$ is a decreasing function of energy in this region of energy. As a result of these differences between data sets 1 and 2, extraction of individual α_1 and α_2 cross sections was feasible only for DS-2.

Figure 1 shows typical spectra at three laboratory angles from DS-2. Proper choice of detector thickness permitted clean separation of the first six alpha groups (α_0–α_5) from the protons produced by the $^{16}O(\alpha, p)^{19}F$ reaction. (Too thick detectors used for DS-1 allowed proton groups to obscure most α_5 peaks and at several angles some α_3 and α_4 peaks.) Thin detectors in a few cases (such as the $\theta_{lab} = 165°$ spectrum in Fig. 1) did not stop completely the elastically scattered alpha particles α_0.

To analyze such a large number of spectra (more than 10 500) some method for automating the extraction of peak yields and their reduction to cross sections was imperative. To this end I developed a computer program[5] that employs the following semiautomatic procedure. During a setup operation the experimenter uses the program to read from magnetic tape and display on a cathode ray tube one spectrum from an angular array (all spectra of which have a common bombarding energy). He uses a light pen to manually adjust a background curve and the limits of integration around the peak of interest. As this procedure is repeated for each spectrum in the angular array, the program stores information enabling it to shift the background curve and limits of integration to account for reaction kinematics and energy loss in the target gas as the bombarding energy changes. Thus, after output of the first angular distribution onto magnetic tape, subsequent spectra are read and displayed with a background curve and integration limits determined from the setup information. If satisfied with the background subtractions, the experimenter merely pushes a sense button to calculate the cross section and proceed to the next spectrum. Adjustments to the background curve or to the integration limits update the setup information. This method proved adequate for spectra that contained isolated peaks superimposed on low backgrounds, and indeed, shortened data reduction time by at least an order of magnitude over previous programs.[5] For the well separated α_0, α_3, α_4, and α_5 groups from both data sets and for the unresolved doublet α_{1+2} group from DS-1, cross sections were calculated using this procedure.

Yields for α_1 and α_2 were extracted from DS-2 spectra by peak fitting techniques. Our standard peak fitting program uses a skewed-Gaussian peak shape which is determined empirically. The program searches on peak amplitudes and on peak widths and/or positions until it cannot produce a significant improvement in the fit as measured by χ^2. In general, one should take advantage of any reliable information which permits reducing the number of adjustable parameters. Fortunately, such information existed in all of the DS-2 spectra in the form of the clearly resolved α_3 and α_4 groups near the α_1 and α_2 doublet. For a given detector in the angular array the width of the α_1 and α_2 peaks differs only by small (and calculable) kinematic broadening effects from the width of the α_3 and α_4 peaks. Furthermore, the separation between the α_1 and α_2 peaks is easily obtained from the known energies of the four alpha groups

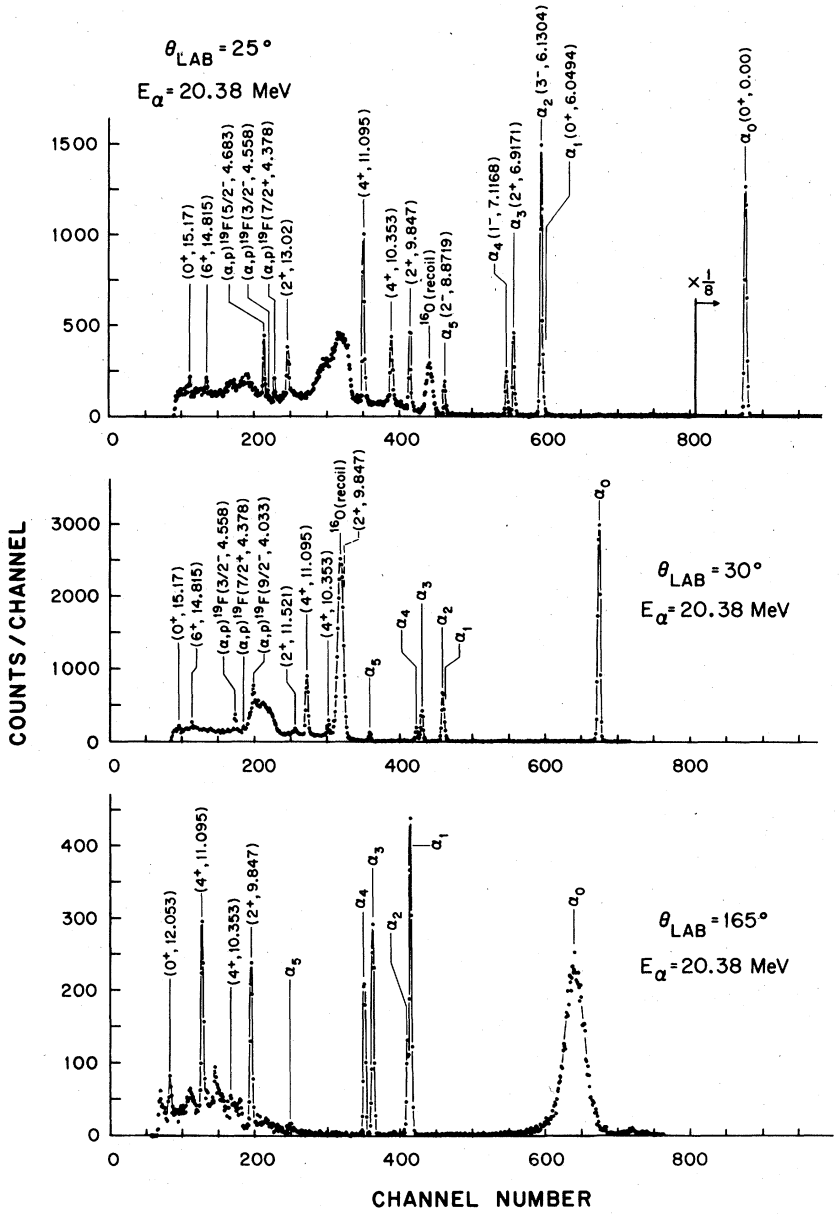

FIG. 1. Sample spectra. This figure shows at three laboratory angles sample spectra collected at $E_\alpha = 20.38$ MeV, the highest alpha energy used in the experiment. Peaks labeled by spin-parity and excitation energy (J^π, E_x) correspond to α groups leading to the indicated ^{16}O final states. The α groups leading to the ground and first five ^{16}O excited states are also labeled by the α_i notation in the $\theta_{lab} = 25°$ spectrum and by only this notation in the $\theta_{lab} = 30°$ and 165° spectra. Proton groups [from the $^{16}O(\alpha,p)^{19}F$ reaction] which were not stopped in the detector contribute to the broad structure at channel 320 and 220 in the $\theta_{lab} = 25°$ and 30° spectra respectively. Elastically scattered alphas were not stopped in the $\theta_{lab} = 165°$ detector. Inelastic alpha groups at least up to $E_x = 15.2$ MeV in ^{16}O may be identified in the $\theta_{lab} = 25°$ and 30° spectra. Broader alpha peaks and those with low yield were obscured by overlapping proton groups and background from other sources, chiefly breakup alphas from ^{16}O continuum states.

and from the α_3 and α_4 peak positions. Again the large number of spectra required automation of the yield extraction procedure. After some initial setup, the peak fitting program extracted the α_1 and α_2 yields for all spectra collected with a common detector in the following manner: First the α_3 and α_4 region of the spectrum was fitted to obtain width and position information for the subsequent α_1 and α_2 fitting procedure. For the fit of α_3 and α_4 the program searched on six param-

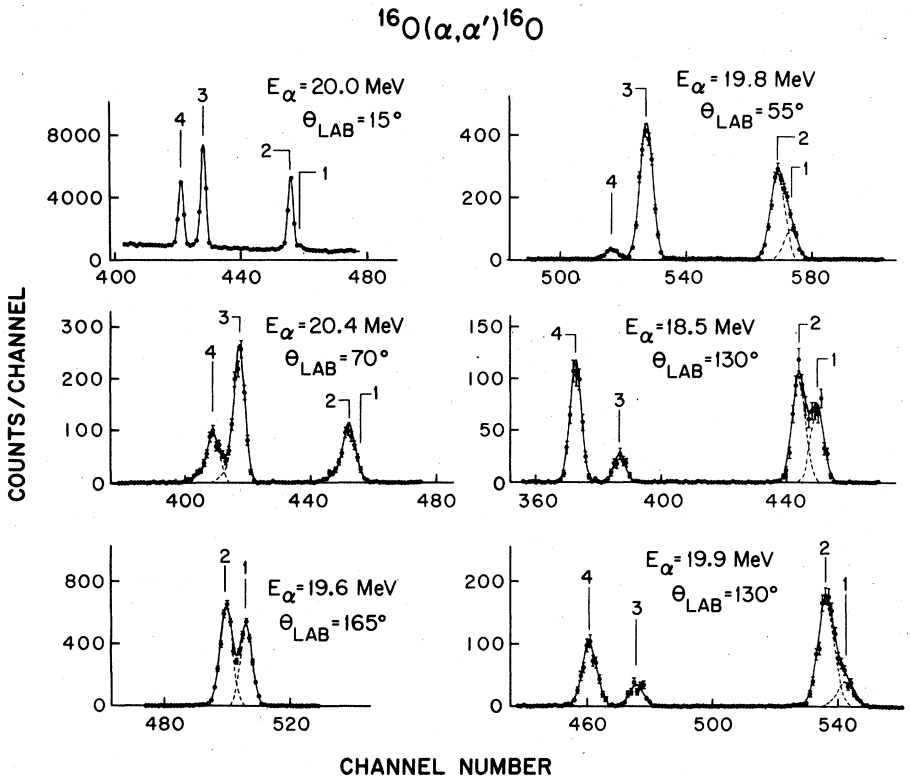

FIG. 2. Sample fitting of spectra results. The vertical lines labeled 1 through 4 indicate the calculated centroids of the α_1 through α_4 peaks. Solid curves are fits obtained by the method described in the text. Dashed curves are individual peak shapes. The separate α_1 and α_2 fit at $\theta_{lab} = 165°$ resulted from a search on the peak width and on both peak positions. The $\theta_{lab} = 70°$ spectrum represents some of our poorest data and shows marginal resolution even of α_3 and α_4 with quite non-Gaussian peak shapes. With proper choice of peak shape parameters all of the $\theta_{lab} = 70°$ spectra were fitted with a mean χ^2/degree of freedom of 1.65.

eters: a single width, the height of a flat background, and the positions and amplitudes of both peaks. After completion of an α_3 and α_4 fit the program used reaction kinematics information read from tape with each spectrum and the results of the fit to set up the fitting region and initial parameters for the α_1 and α_2 fit. For this fit the width and separation of the peaks were fixed. The program searched only on the position of the taller of the two peaks, the background height, and the peak amplitudes. At the end of an α_1 and α_2 fit the program wrote on magnetic tape the calculated yields of the alpha groups, then proceeded automatically to the next spectrum for the same laboratory angle. Using the results of the previous α_3 and α_4 fit the program adjusted the peak positions and fitting region to account for the difference in bombarding energy. The initial width was set equal to the last α_3 and α_4 width. In this fully automatic mode the fitting program usually obtained good fits after only one or two iterations and was often unable to improve on the initial set of α_1 and α_2 parameters.

We used this technique to fit the α_1 and α_2 peaks in more than 4000 spectra obtaining a mean χ^2/degree of freedom of 1.48. Figure 2 illustrates sample fits for a few laboratory angles and bombarding energies. For spectra at three laboratory angles (145°, 165°, and 170°) resolution of the α_1 and α_2 groups was good enough so that there was a pronounced dip between the peaks. In those cases it was unnecessary to first fit the α_3 and α_4 peaks and we allowed the fitting program to search on the positions of both α_1 and α_2. The $\theta_{lab} = 165°$ spectrum shown in Fig. 2 was fit in this manner. Typically, the α_1 yield was less than the α_2 yield in the energy range $18.0 \leq E_\alpha \leq 20.4$ MeV.

Uncertainties arising from random errors other than statistical errors are typically 2% for all of the cross sections from both data sets.[5] Statistical errors vary widely for the different reactions and, of course, depend on the yield. For elastic scattering the statistical errors range from 0.6% to 3%; for α_3 and α_4 they range from 2% to 8%. The α_5 cross sections have statistical

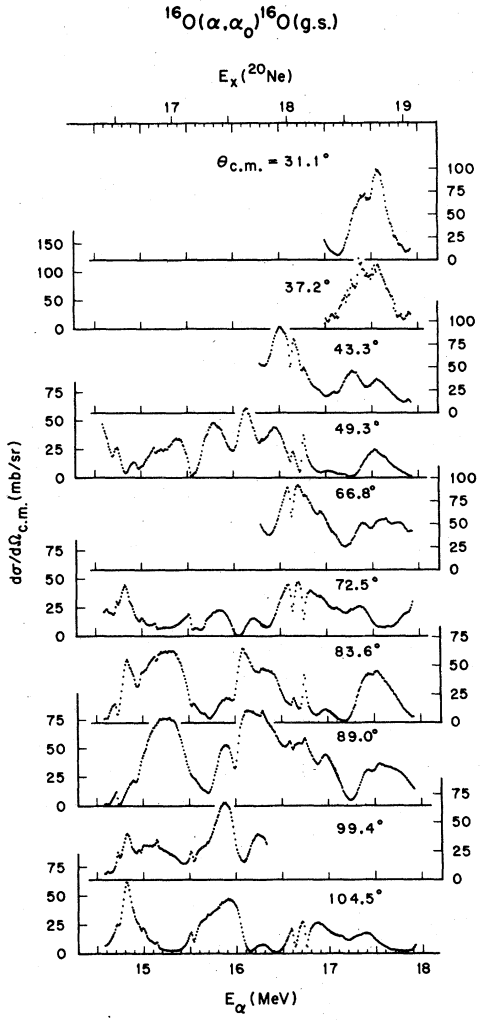

FIG. 3. $^{16}O(\alpha,\alpha_0)^{16}O$ differential cross sections for ten laboratory angles (θ_{lab}=25°, 30°, 35°, 40°, 55°, 60°, 70°, 75°, 85°, 90°) in the bombarding energy range 14.6 $\leq E_\alpha \leq$ 18.0 MeV.

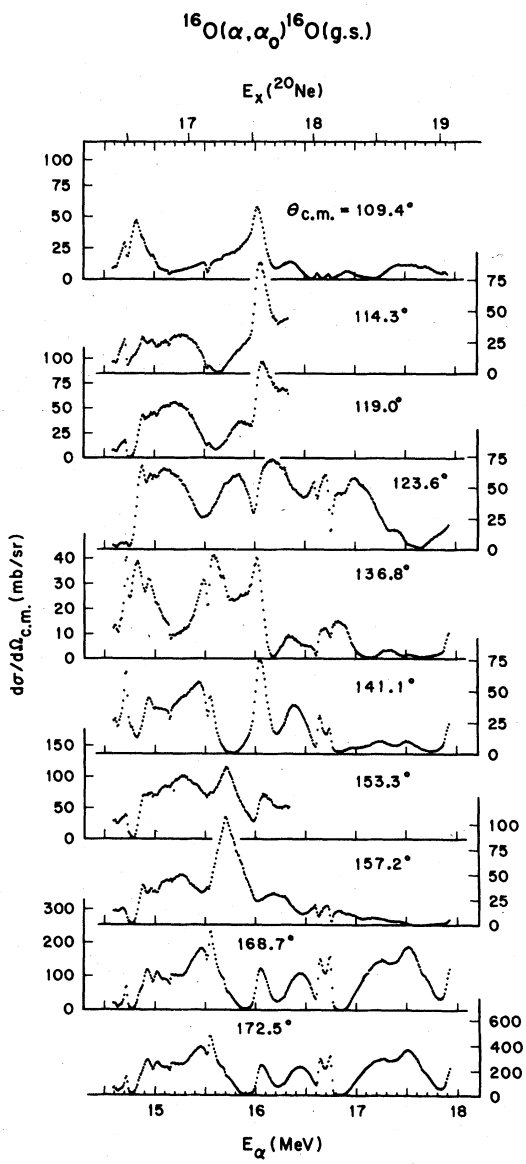

FIG. 4. $^{16}O(\alpha,\alpha_0)^{16}O$ differential cross sections for ten laboratory angles (θ_{lab}=95°, 100°, 105°, 110°, 125°, 130°, 145°, 150°, 165°, 170°) in the bombarding energy range 14.6 $\leq E_\alpha \leq$ 18.0 MeV.

errors of the order of 5% except at extreme forward and backward angles where the errors may rise to 20%. (Decay by alpha emission to ^{16}O states of unnatural parity is forbidden at $\theta_{c.m.} = 0°$ and 180°.) For DS-1 the unresolved α_{1+2} cross sections have statistical errors between 1% and 3%. For the α_1 and α_2 groups (whose yields were extracted by peak fitting) each uncertainty consists of the statistical error weighted by χ^2 plus a "background" component which is related to the number of counts in the adjacent α_1 (or α_2) peak. By fitting several spectra many times, each time with slightly different initial amplitudes and positions for the α_1 and α_2 peaks, we found that the scatter in the resulting yields was better approximated by the weighted statistical error plus background component than by the weighted statistical error alone. This approximation most affects the α_1 errors since the α_2 yield was typically much larger than the α_1 yield. The α_1 uncertainties range from 5% to 8% or ~0.1 mb/sr for very small yields. For α_2 cross sections the range is 1.5% to 4%.

Effects of beam heating in the target gas may cause systematic reduction of the cross section measurements and has been discussed by Rose[6] and Pledger.[7] While we did not correct the data

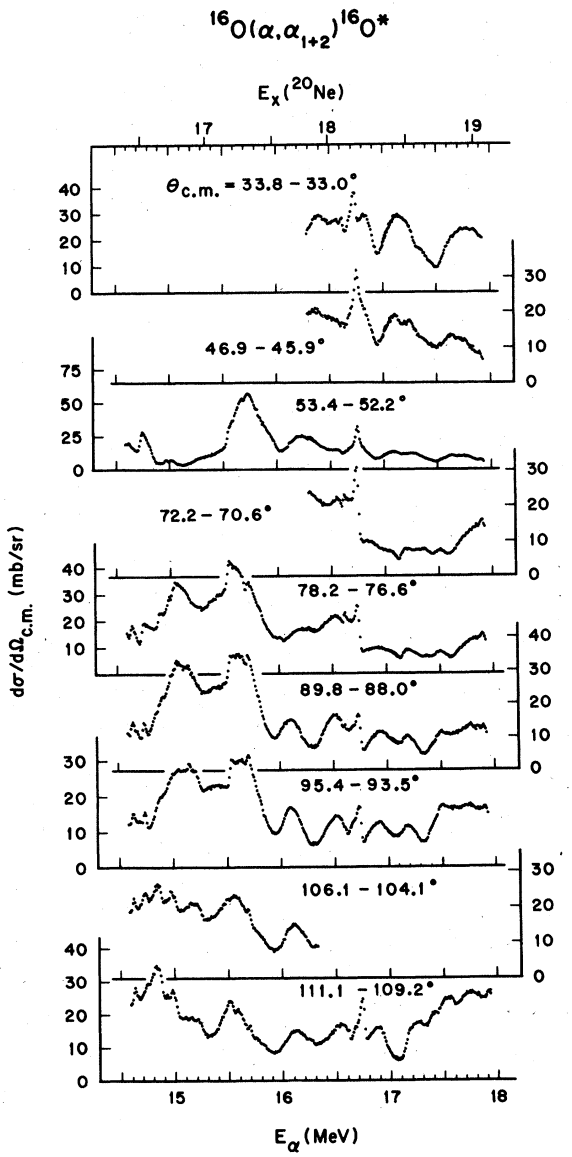

FIG. 5. $^{16}O(\alpha,\alpha_{1+2})^{16}O$ differential cross sections for nine laboratory angles (θ_{lab}=25°, 35°, 40°, 55°, 60°, 70°, 75°, 85°, 90°) in the bombarding energy range 14.6 $\leq E_\alpha \leq$18.0 MeV.

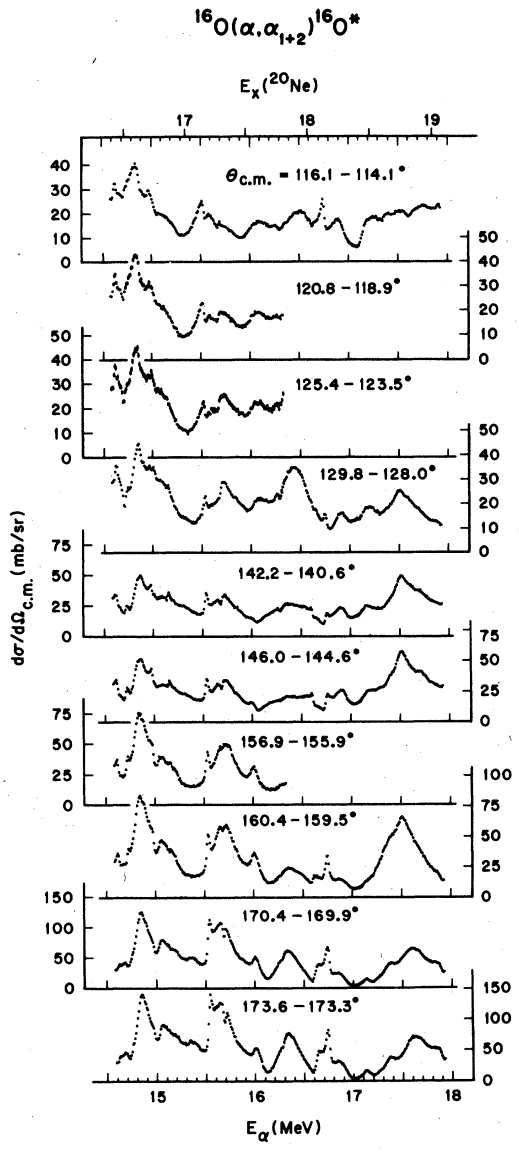

FIG. 6. $^{16}O(\alpha,\alpha_{1+2})^{16}O$ differential cross sections for ten laboratory angles (θ_{lab}=95°, 100°, 105°, 110°, 125°, 130°, 145°, 150°, 165°, 170°) in the bombarding energy range 14.6 $\leq E_\alpha \leq$18.0 MeV.

for such effects, we estimate an upper limit of −2.0% for DS-1 and of −0.75% for DS-2. A recent calibration using threshold energies of several (p,n) reactions, the threshold energy of the $^{12}C(\alpha,n)$ reaction, and the resonant energy of an $^{16}O(p,p)$ resonance near $E_p = 12.7$ MeV determined the absolute energy to better than ± 10 keV for the range of energies covered in this experiment. Even though our 90° magnet's object and image slit separations allow a maximum ±30 keV wander in the beam energy, the observed reproducibility of sharp resonant structures in excitation functions was approximately ±3 keV.

III. RESULTS

Figures 3 through 10 show our differential cross sections from DS-1 for the reactions $^{16}O(\alpha,\alpha_0)^{16}O$, $^{16}O(\alpha,\alpha_{1+2})^{16}O$, $^{16}O(\alpha,\alpha_3)^{16}O$, and $^{16}O(\alpha,\alpha_4)^{16}O$. The lower energy scale in all figures is the laboratory beam energy at the center of the scattering chamber. Excitation energies in ^{20}Ne ($Q = 4.73$ MeV) can be found on the upper energy scale. Except for elastic scattering, the center of mass angles (corresponding to the fixed laboratory angles at which the data were taken) depend on the

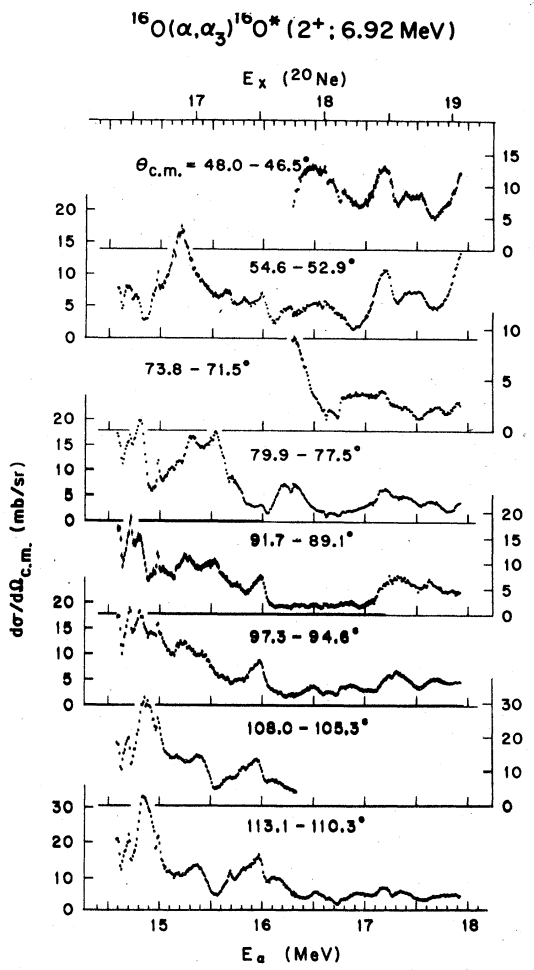

FIG. 7. $^{16}O(\alpha, \alpha_3)^{16}O$ differential cross sections for eight laboratory angles (θ_{lab} = 35°, 40°, 55°, 60°, 70°, 75°, 85°, 90°) in the bombarding energy range $14.6 \leq E_\alpha \leq 18.0$ MeV.

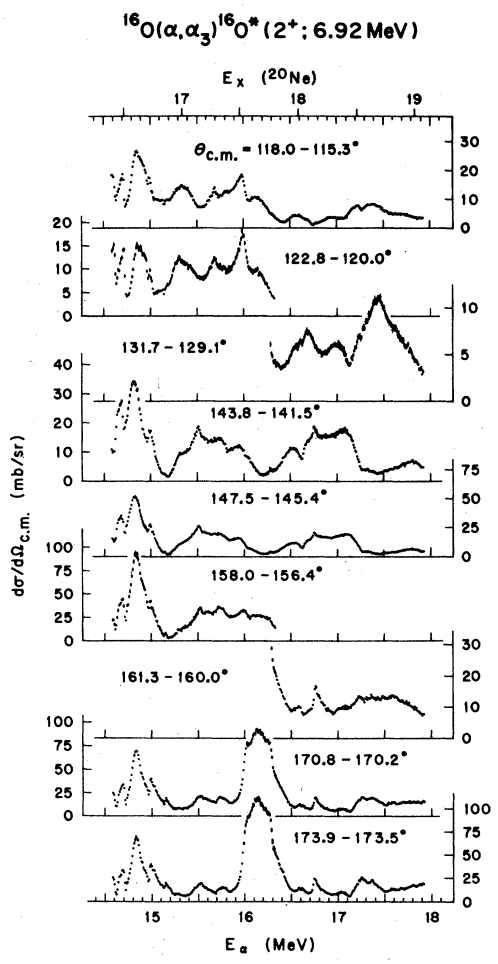

FIG. 8. $^{16}O(\alpha, \alpha_3)^{16}O$ differential cross sections for nine laboratory angles (θ_{lab} = 95°, 100°, 110°, 125°, 130°, 145°, 150°, 165°, 170°) in the bombarding energy range $14.6 \leq E_\alpha \leq 18.0$ MeV.

bombarding energy. The variation in the center of mass angle from the lowest to the highest alpha energy is indicated on each excitation function. Error bars from counting statistics and background subtraction are shown whenever they exceed the point size. The several incomplete excitation functions in these data resulted when four detectors were moved to different laboratory angles. For each bombarding energy we have data at no more than 16 laboratory angles for DS-1. We have no α_3 or α_4 cross sections for $\theta_{lab} = 25°$, 30°, and 105° because too thick detectors at these angles stopped protons with energies comparable to the α_3 and α_4 energies.

Häusser *et al.*[3] have published, for six angles $^{16}O(\alpha, \alpha_0)$ and for three angles $^{16}O(\alpha, \alpha_{1+2})$, excitation functions covering the energy range $14.2 \leq E_\alpha \leq 17.2$ MeV. We compared their α_0 data at $\theta_{c.m.} = 123.6°$ to our α_0 data at the same angle. The locations of sharp structures in the excitation plots indicated that our energies are about 14 keV lower than Chalk River's near 14.8 MeV but agree to within ±8 keV above 15.9 MeV. In relatively flat regions our cross sections exceed those of the Chalk River group by 5% at 15.10 MeV, 2% at 16.17 MeV, and 3% at 16.82 MeV. Other excitation functions at center of mass angles differing by only 2° to 6° from those of Häusser *et al.* agreed qualitatively for both the α_0 and the α_{1+2} reactions. The Chalk River group used a solid WO_3 target and obtained the differential cross sections by assuming Rutherford cross sections for the elastic scattering from W.

The only other extensive work that overlaps our DS-1 is the $^{16}O(\alpha, \alpha_0)^{16}O$ data of Mehta, Hunt, and Davis[2] (MHD) who published excitation curves for eight angles in energy steps of 50 keV. Though

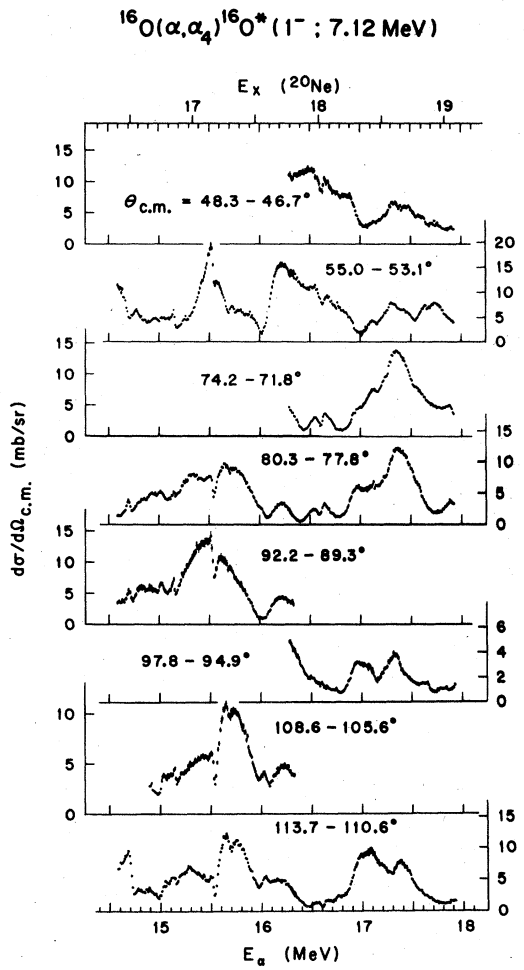

FIG. 9. $^{16}O(\alpha,\alpha_4)^{16}O$ differential cross sections for eight laboratory angles (θ_{lab} = 35°, 40°, 55°, 60°, 70°, 75°, 85°, 90°) in the bombarding energy range 14.6 $\leq E_\alpha \leq$ 18.0 MeV.

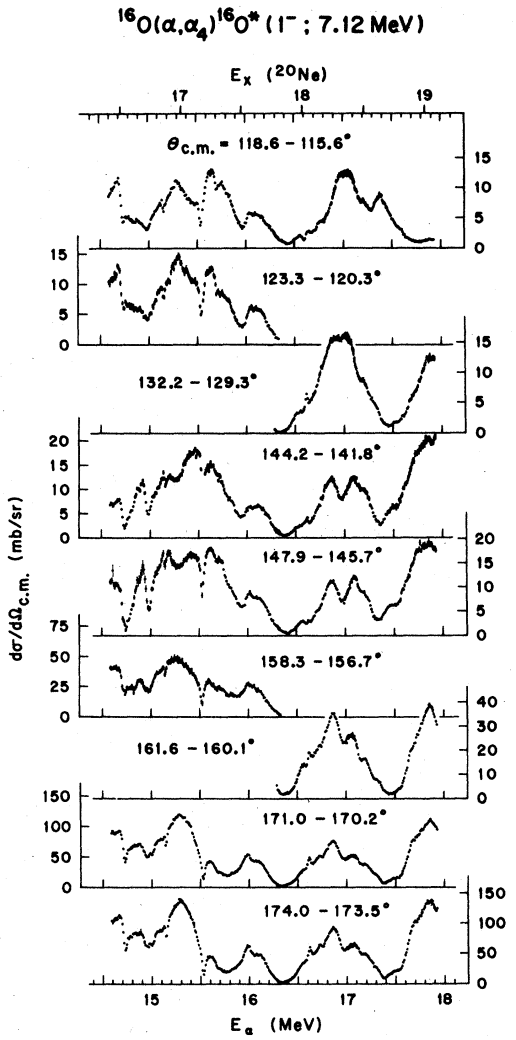

FIG. 10. $^{16}O(\alpha,\alpha_4)^{16}O$ differential cross sections for nine laboratory angles (θ_{lab} = 95°, 100°, 110°, 125°, 130°, 145°, 150°, 165°, 170°) in the bombarding energy range 14.6 $\leq E_\alpha \leq$ 18.0 MeV.

qualitatively similar in shape, our α_0 cross sections are ~40% larger than those of MHD. John *et al.*[8] whose data overlapped the MHD data between E_α = 10.0 and 12.5 MeV also observed such a discrepancy and attribute it to the fact that MHD could not determine accurately the thickness of their SiO_2 targets.

Figures 11 through 14 present the DS-2 differential cross sections for elastic scattering and for inelastic scattering to the first excited state of ^{16}O at E_x = 6.05 MeV. These figures show the data for the scan in 10-keV steps from E_α = 18.0 to 20.4 MeV. They do not include data at five laboratory angles (θ_{lab} = 10°, 20°, 125°, 155°, and 165°) over the same energy range but collected in steps of 10 to 30 keV. For the α_1 reaction Figs. 15 and 16 give the coefficients of the Legendre polynomial expansion

$$\left.\frac{d\sigma}{d\Omega}\right|_{c.m.} = \sum_{\nu=0}^{\nu_{max}} a_\nu P_\nu(\cos\theta) . \quad (1)$$

For the other inelastic reactions (α_2, α_3, α_4, and α_5) Figs. 17 through 24 display the data in terms of Legendre coefficients. Numerical values of all the cross sections (including those not shown) and of the Legendre coefficients are available from the American Institute of Physics depository service (PAPS).[9]

For the Legendre polynomial fitting we used 21-point angular distributions which consisted of the 18 point distributions from our 10-keV step excitation functions plus cross sections at laboratory angles of 10°, 20°, and 155° interpolated in energy from the scan of the same region taken in steps

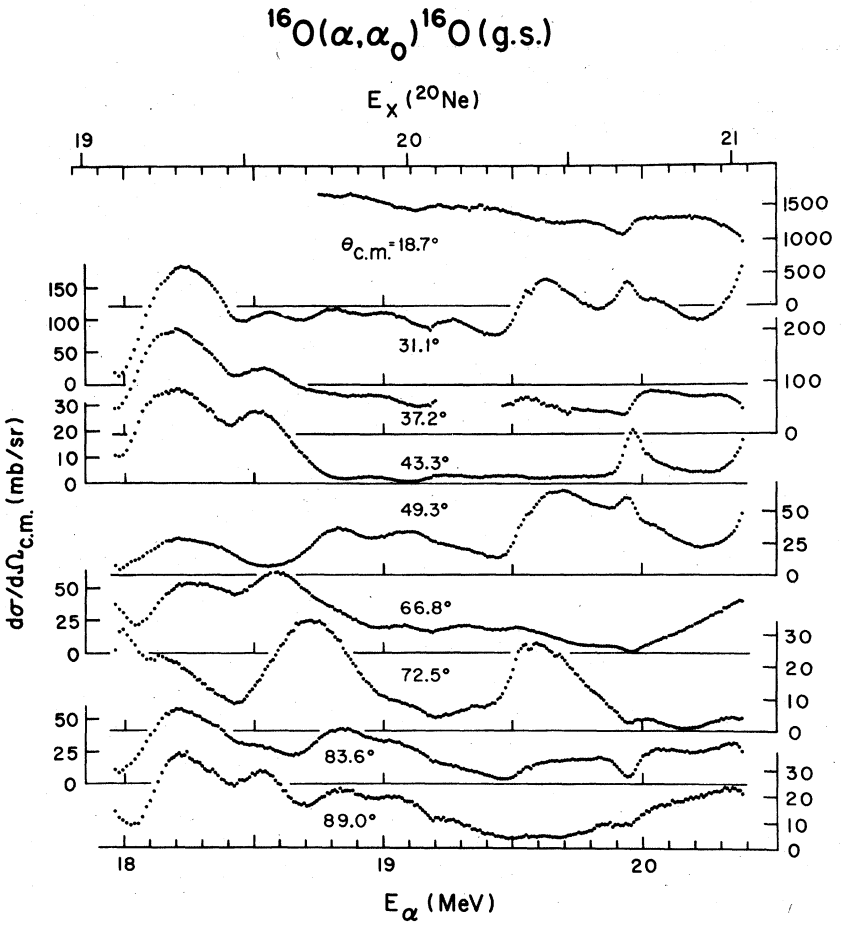

FIG. 11. $^{16}O(\alpha,\alpha_0)^{16}O$ differential cross sections for nine laboratory angles (θ_{lab}=15°, 25°, 30°, 35°, 40°, 55°, 60°, 70°, 75°) in the bombarding energy range $18.0 \leq E_\alpha \leq 20.4$ MeV.

of 10 to 30 keV. (We used 10-keV steps for these data near $E_\alpha = 20$ MeV where the cross sections exhibited sharp structure and 20- or 30-keV steps elsewhere.) For each of the three angles we applied a quadratic interpolating polynomial[10] to the three cross section measurements closest to the required energy of the 18-point distribution. We found good agreement (within statistical errors) between interpolated cross sections and measured cross sections when the method was applied to data for two laboratory angles common to both scans of the energy region. Including the forward angle data in the calculation of Legendre expansions reduced greatly uncertainties in the coefficients a_ν and also eliminated unphysical behavior (negative values) of the cross sections when extrapolated toward $\theta_{c.m.} = 0°$.

We calculated the Legendre expansion for each angular distribution for several different maximum orders ν_{max}. The best fit corresponds to the lowest ν_{max} for which the confidence level (CL) is between 0.1 and 0.9. For the α_2, α_3, and α_4 reactions the optimum choice was $\nu_{max} = 14$ over the entire energy range from $E_\alpha = 18.0$ to 20.4 MeV. A maximum order of $\nu_{max} = 14$ was also sufficient for E_α between 18.0 and 18.8 MeV for the α_1 reaction; $\nu_{max} = 15$ was required for $E_\alpha > 18.8$ MeV. For the α_5 reaction the CL criterion needed only $\nu_{max} = 13$ for $E_\alpha < 18.7$ MeV and $\nu_{max} = 12$ for $E_\alpha > 18.7$ MeV.

One interesting feature of the Legendre coefficients is the tendency for adjacent-order coefficients to mirror one another over wide energy ranges. The effect is most evident in the α_1 and α_4 Legendre coefficients (see Figs. 15, 16, 21, and 22) and to a lesser extent in the α_5 coefficients (Figs. 23 and 24). For these cases the a_{even} coefficients are usually positive while the adjacent a_{odd} terms are negative and of similar magnitude. In Fig. 15 for the α_1 reaction note the behavior of a_1 and a_2 over most of the energy range. The mirror effect is even more persistent for the α_4

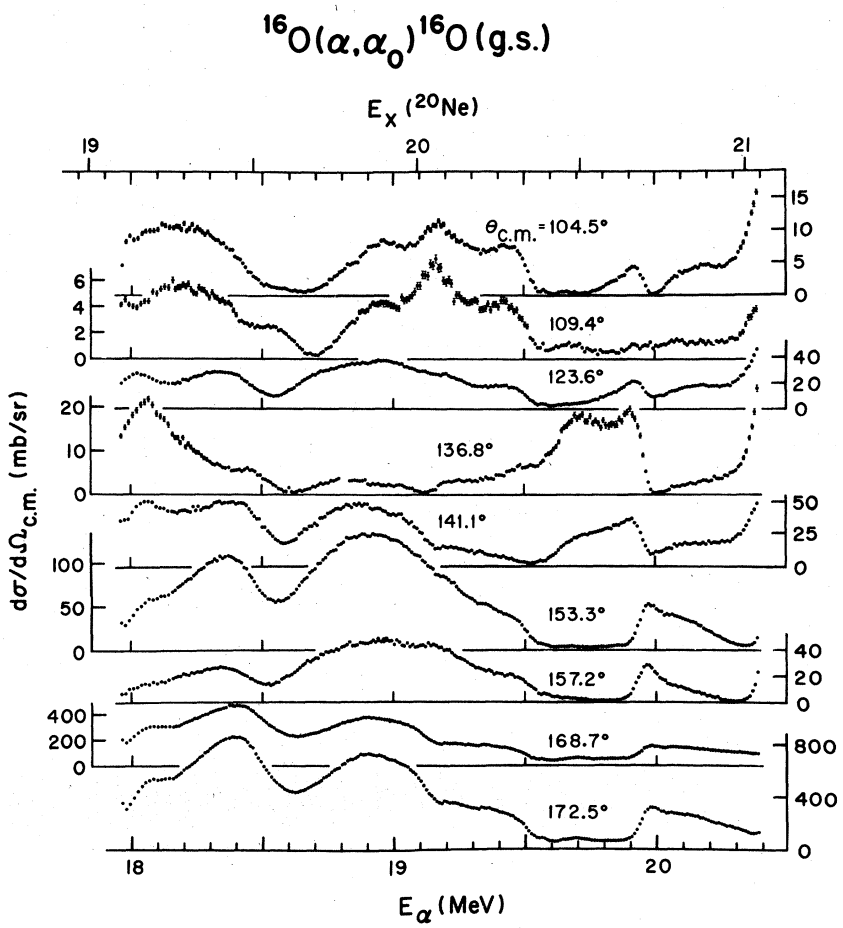

FIG. 12. $^{16}O(\alpha,\alpha_0)^{16}O$ differential cross sections for nine laboratory angles (θ_{lab} = 90°, 95°, 110°, 125°, 130°, 145°, 150°, 165°, 170°) in the bombarding energy range $18.0 \leq E_\alpha \leq 20.4$ MeV.

coefficients shown in Figs. 21 and 22. I am not aware of any property of the angular distribution or of the reaction mechanism which should produce this rather striking behavior.

Except for the α_1 reaction, the expansions in terms of Legendre polynomials represent the extent of our analysis of the inelastic scattering data. Friedman has indicated,[11] however, that some of the resonant structures observed in the inelastic scattering excitation functions can be understood in terms of an excited-core model of the nucleus.

For our DS-2 the α_0 cross sections also overlapped the MHD[1] data in the energy range $18.0 \leq E_\alpha \leq 19.0$ MeV. As with our lower energy data, these cross sections were also significantly larger than those reported by MHD. Above $E_\alpha = 19$ MeV our data overlapped the α_0 and α_{1+2} data of Bergman and Hobbie[2] (BH) which consisted of excitation functions at eight angles in steps of 20 keV. None of our center of mass angles correspond exactly with those of BH, but at three angles of near overlap ($\leq 1.0°$) the cross sections agree to within ± 6%. There appears to be a larger discrepancy between the MHD data and the BH data than the 10% mentioned by BH in their paper.[2] The only other published data that overlaps the present work is from the very early study of Corelli *et al.*[4] These α_0, α_{1+2}, and α_{3+4} data show only a vague qualitative resemblance to ours.[5]

IV. ANALYSIS

The most complete description of the scattering process involves specification of the S matrix. However, the complication introduced by nonzero spin in the residual nucleus precludes for all but the simplest cases determination of the S-matrix elements from differential cross section data alone. The six different reactions studied in this experiment all involve spinless positive-parity

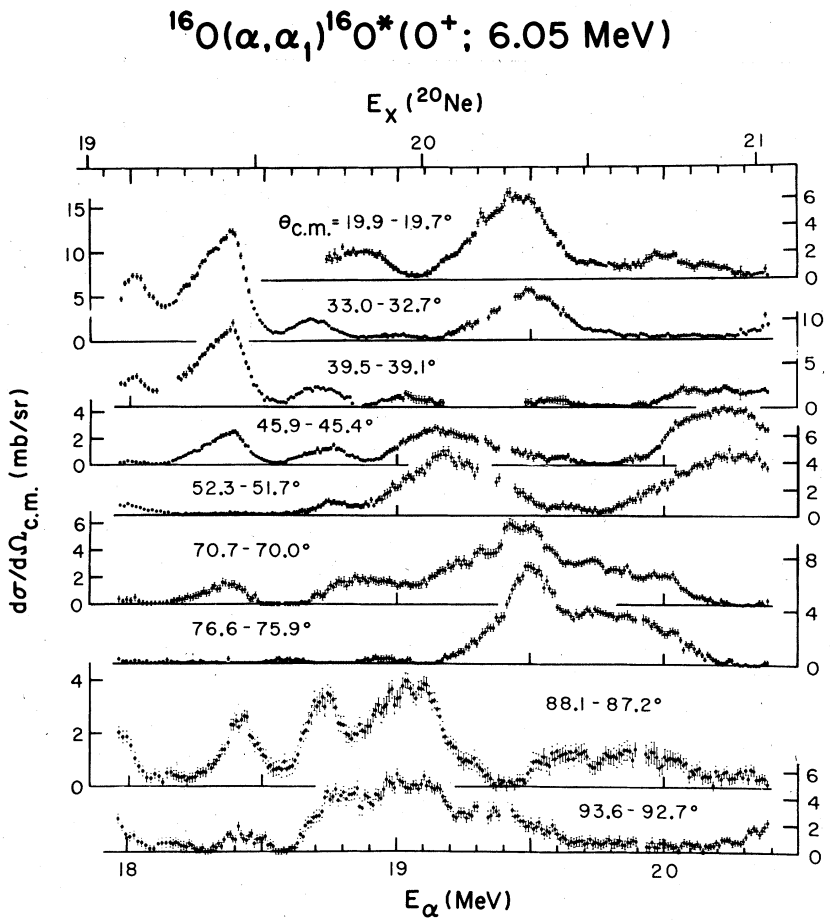

FIG. 13. $^{16}O(\alpha,\alpha_1)^{16}O$ differential cross sections for nine laboratory angles (θ_{lab}=15°, 25°, 30°, 35°, 40°, 55°, 60°, 70°, 75°) in the bombarding energy range $18.0 \leq E_\alpha \leq 20.4$ MeV.

(0^+) particles in the incident channel and at least one 0^+ particle in the outgoing channel:

$$0^+ + 0^+ \rightarrow 0^+ + I^\pi,$$

where I^π is the spin and parity of the final state reached in the residual ^{16}O nucleus. Though the reaction amplitude[12] describing the angular distribution of the cross section undergoes considerable simplification for this class of spin systems, the problem is tractable only for $I^\pi = 0^+$ or 1^+ ($I^\pi = 0^-$ is forbidden by parity conservation). The case of all spinless particles ($I^\pi = 0^+$) is, of course, well known and requires the determination of $(l_{max}+1)$ S-matrix elements, where l_{max} is the quantum number of the largest orbital angular momentum contributing to the scattering amplitude. Jolivette and Richards[13] carried out the reduction of the general equations (3.13)–(3.16) of Ref. 12 for the case $I^\pi = 1^+$. The resulting expression[13] involves only l_{max} different S-matrix elements ($l = J = 0$ is forbidden) so that, in a sense, this case is simpler than the case of all spinless particles. Table I shows the requisite number of matrix elements S_l^J, for values of I^π as a function of l_{max} in order of increasing complexity. To illustrate the degree of increased complexity consider the $I^\pi = 2^-$ case (next simplest after $I^\pi = 1^+$ and 0^+). The scattering amplitude [see Eq. (3.14) of Ref. 12] reduces to the form

$$q(\theta,\phi) = q_+ + q_-, \tag{2}$$

$$q_\pm = \sum_{l=0}^{l_{max}} \pm i\pi^{1/2}(2l+1)^{1/2}(l \pm 1\ 2\ -m_s'\ m_s'|l\ 0)S_{l\pm1}^{l}Y_{l\pm1}^{-m_s'}.$$

Evaluation of the differential cross section still involves summing over the allowed outgoing channel spin projections $m_s' = \pm1, \pm2$, ($m_s' = 0$ is forbidden). Thus the final expression includes terms containing both first and second derivatives of the Legendre polynomials.

To analyze our data for the two reactions having $I^\pi = 0^+$ (α_0 and α_1) we used a method first described

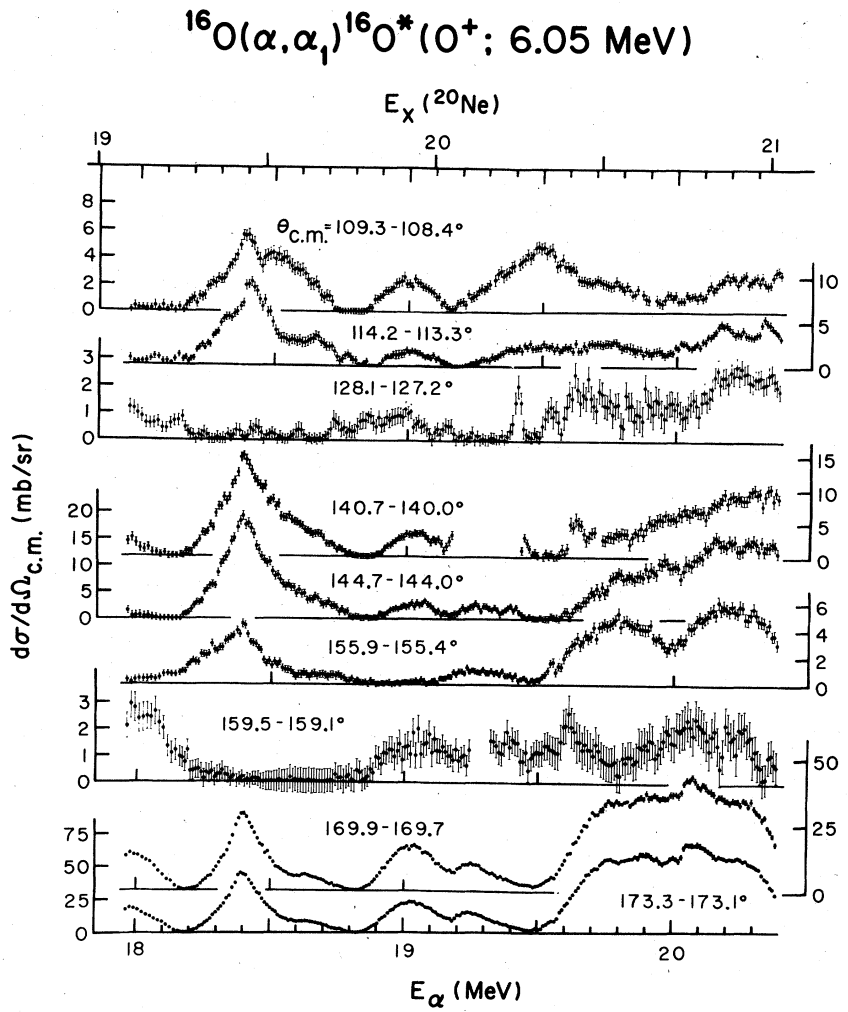

FIG. 14. $^{16}O(\alpha,\alpha_1)^{16}O$ differential cross sections for nine laboratory angles (θ_{lab}=90°, 95°, 110°, 125°, 130°, 145°, 150°, 165°, 170°) in the bombarding energy range $18.0 \leq E_\alpha \leq 20.4$ MeV.

TABLE I. Number of scattering matrix terms in the reaction amplitude for the spin system: $0^+ + 0^+ \rightarrow 0^+ + I^\pi$ (l and l' label incoming and outgoing orbital angular momenta).

I^π	Number of $S_{l'}^{l}$
1^+	l_{max}
0^+	$l_{max}+1$
2^-	$2l_{max}-1$
1^-	$2l_{max}+1$
3^+	1, for $l_{max}=1$ $3l_{max}-3$, for $l_{max}\geq 2$
2^+	1, for $l_{max}=0$ $3l_{max}$, for $l_{max}\geq 1$
3^-	$2l_{max}+1$, for $l_{max}\leq 1$ $4l_{max}-2$, for $l_{max}\geq 2$

by Häusser *et al.*[3] in which one writes the scattering amplitude as a nonresonant term plus a sum over only resonant partial waves. One starts with the usual expansion[12] in partial waves of the scattering amplitude $f(\theta)$ for spinless particles

$$\frac{d\sigma}{d\Omega}(\theta, E) = |f(\theta)|^2,$$

$$f(\theta) = f_C(\theta) + \frac{i}{2k}\sum_l (2l+1)\exp(2i\alpha_l) \times (1-S_l)P_l(\cos\theta), \quad (3)$$

$$S_l = \exp(2i\phi_l)\left\{\frac{\Gamma_{\alpha_i}}{\Gamma}[\exp(2i\beta_l)-1]+1\right\},$$

where $f_C(\theta)$ is the Coulomb amplitude, α_l is the relative Coulomb phase shift, S_l are elements of

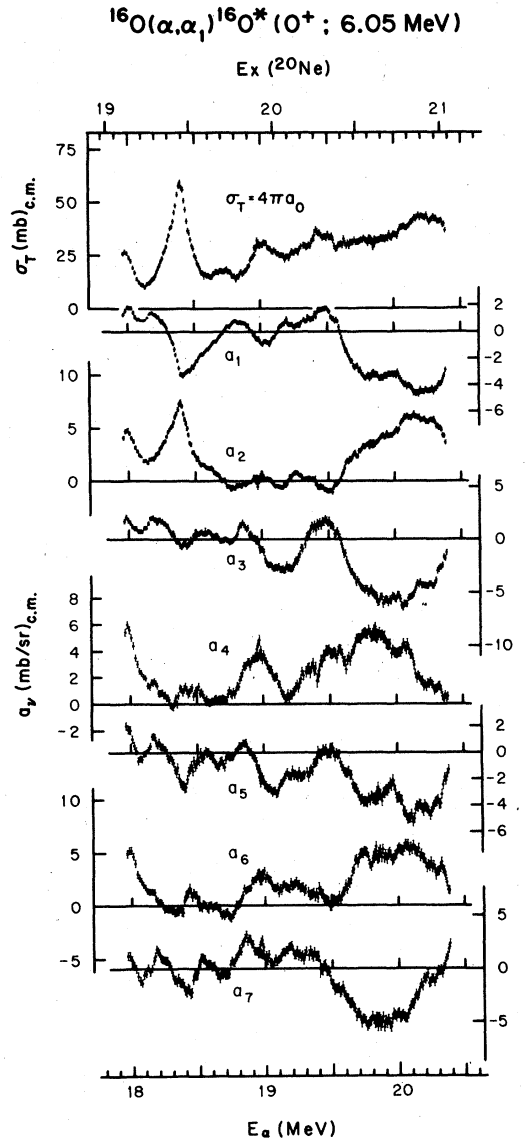

FIG. 15. Lower order coefficients of the Legendre polynomial expansion as a function of bombarding energy for the reaction $^{16}O(\alpha,\alpha_1)^{16}O$.

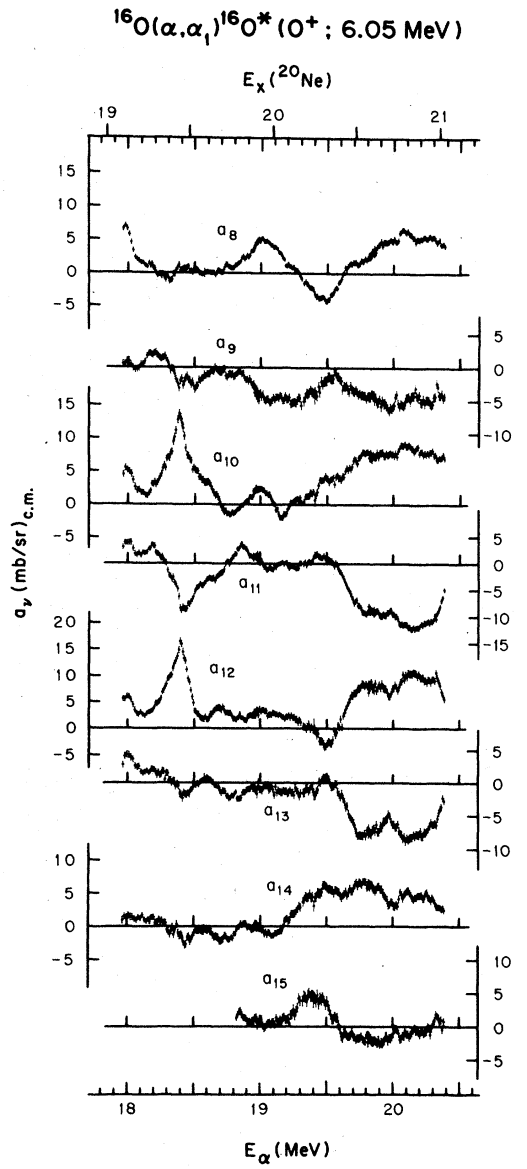

FIG. 16. Higher order Legendre coefficients for the reaction $^{16}O(\alpha,\alpha_1)^{16}O$.

the scattering matrix S, Γ is the total resonant width, Γ_{α_i} is the partial width for a given reaction channel, and ϕ_l is the nonresonant part of the total nuclear phase shift. The resonant phase shift is given by

$$\beta_l = \tan^{-1}\left(\frac{\Gamma/2}{E_r - E}\right), \tag{4}$$

where E is the bombarding energy and E_r is the resonant energy associated with partial wave l. [For a single open channel $\Gamma_{\alpha i} = \Gamma$ and the expression for S_l reduces to the familiar $\exp(2i\delta_l)$, where δ_l is the total nuclear phase shift.] Next, one combines with the Coulomb term each nonresonant partial wave's contribution to the summation in Eq. (3). Furthermore, for the resonant partial waves one also combines with this nonresonant term the two terms not containing $[\exp(2i\beta_l) - 1]$. The result is the following formula for the differential cross section:

$$\frac{d\sigma}{d\Omega}(\theta, E) = \Big| \rho(\theta)\exp[i\chi(\theta)] + \frac{i}{2k}\sum_{l=l_r}(2l+1)\frac{\Gamma_{\alpha i}}{\Gamma}[\exp(2i\beta_l) - 1] \times \exp[2i\phi_l'(\theta)]P_l(\cos\theta)\Big|^2, \tag{5}$$

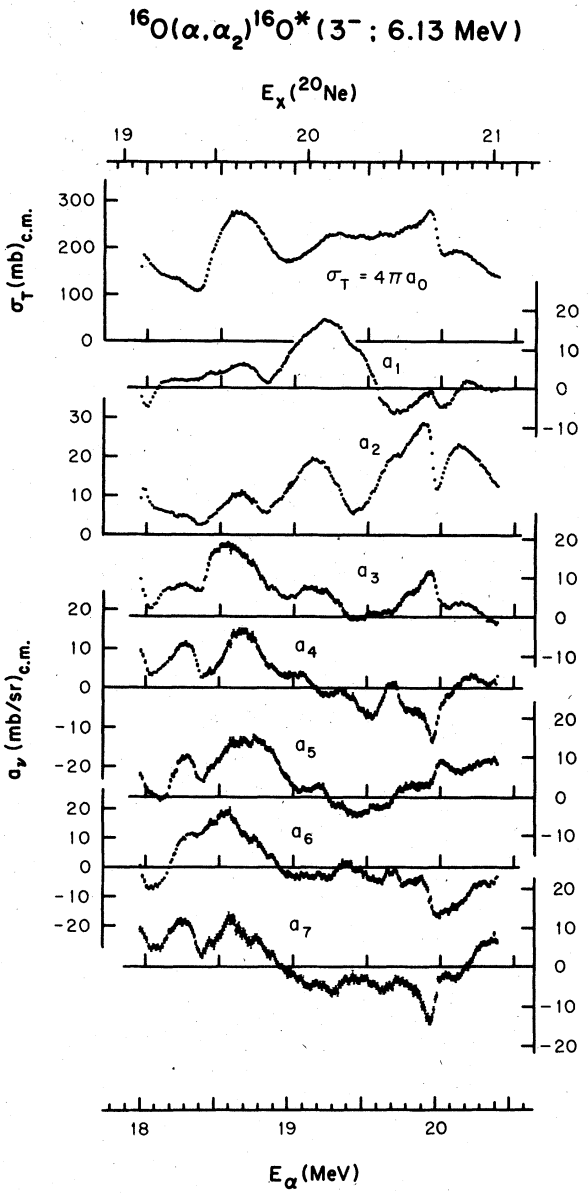

FIG. 17. Lower order coefficients of the Legendre polynomial expansion as a function of bombarding energy for the reaction $^{16}O(\alpha, \alpha_2)^{16}O$.

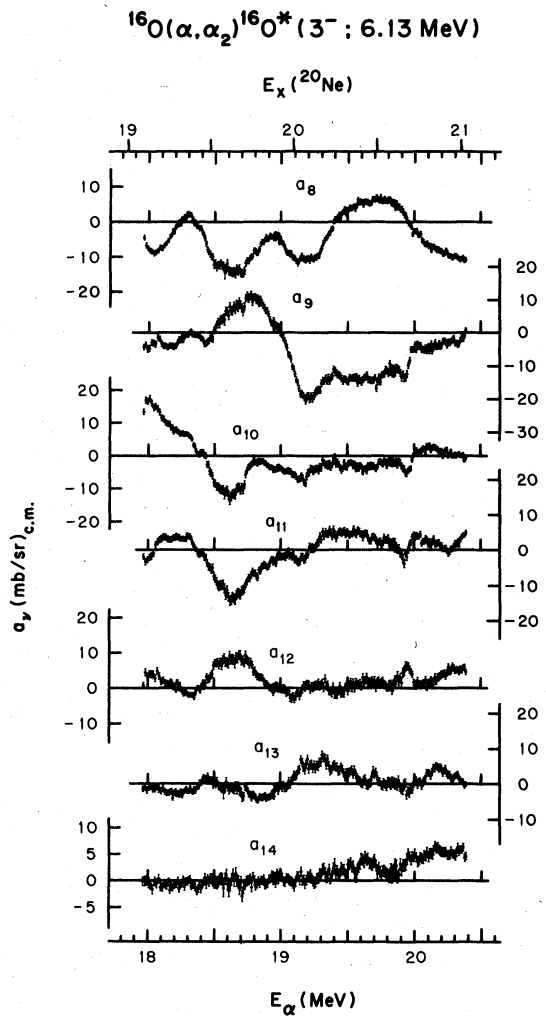

FIG. 18. Higher order Legendre coefficients for the reaction $^{16}O(\alpha, \alpha_2)^{16}O$.

where $\rho(\theta)$ is the nonresonant amplitude which over the fitting region we assume varies only linearly with energy, $\chi(\theta)$ is the phase of the nonresonant term, and $\phi_l'(\theta)$ are nonresonant background phases which we assume also vary linearly with energy. The indicated summation is over only resonant partial waves. In actual computations with Eq. (5) there is one overall arbitrary phase for each angle θ. Thus if one sets $\exp[i\chi(\theta)] = 1$ only the relative phase between each resonant term and the nonresonant amplitude need be determined. The parameters $\phi_l'(\theta)$ along with $\rho(\theta)$ were fitted separately at each angle θ. A total of 1000 datum points (50 energies at 20 angles) may be fit simultaneously using a program developed to run on our DDP-124 computer. A fitting function may include up to five resonant terms. As computation time increased rapidly for larger data sets and more resonances we attempted where possible to focus on small portions of the excitation function. A more detailed discussion of the resonance fitting procedure may be found in Ref. 5.

According to McDermott *et al.*[14] the correct form for the resonant phase in the case of two overlapping levels of the same spin and parity is:

$$\beta_l = \tan^{-1}\left[\frac{1}{C_l + \left(\frac{\Gamma_1/2}{E_1 - E} + \frac{\Gamma_2/2}{E_2 - E}\right)^{-1}}\right], \qquad (6)$$

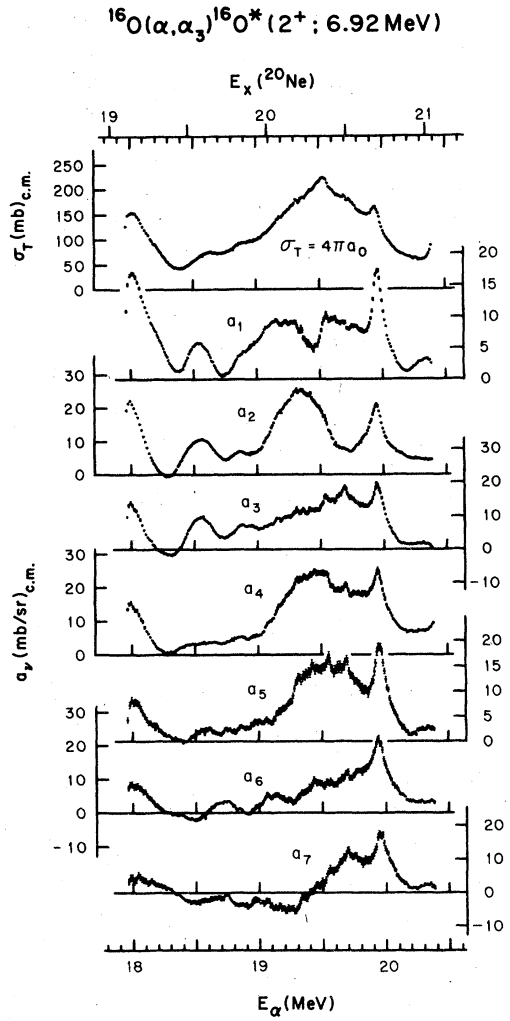

FIG. 19. Lower order coefficients of the Legendre polynomial expansion as a function of bombarding energy for the reaction $^{16}O(\alpha,\alpha_3)^{16}O$.

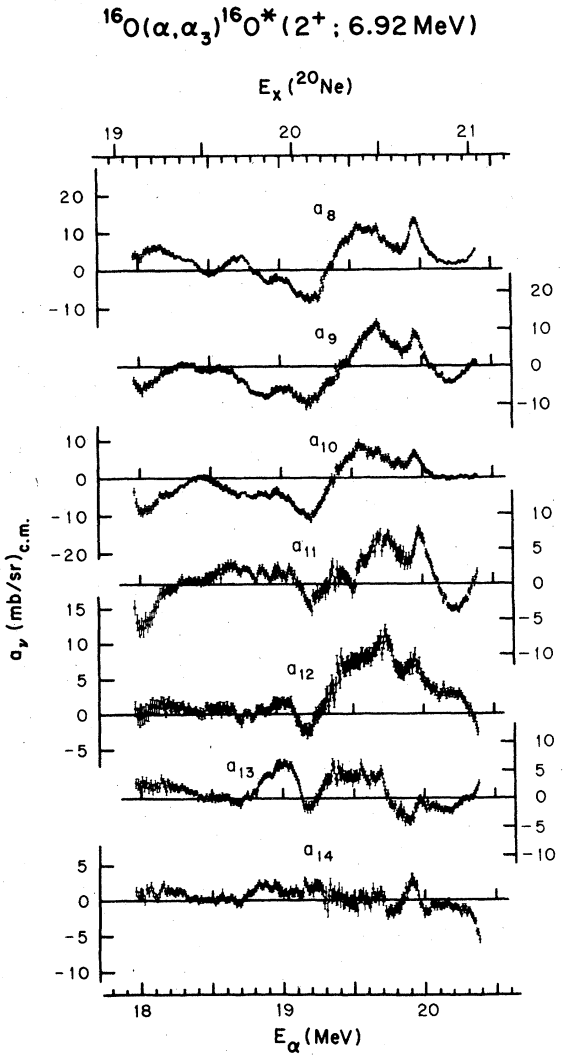

FIG. 20. Higher order Legendre coefficients for the reaction $^{16}O(\alpha,\alpha_3)^{16}O$.

where Γ_1 and Γ_2 are the resonant widths and E_1 and E_2 are the corresponding resonant energies. Steck[15] showed that different choices for the coupling parameter C_l could alter considerably the shape of the excitation function depending upon the relative level widths and upon the energy spacing. The complication and extra parameter C_l introduced by including the interference effects of nearby levels of the same J^π made this approach not feasible for our type of analysis. While we may miss a particular level whose presence is masked by interference effects, it is not possible for a single level to mimic two interfering levels. Thus, if we *do* observe two nearby levels of the same J^π, our analysis may at worst provide incorrect resonant energies and/or widths.

[The above discussion presumes an R-matrix approach to the scattering problem. Instead we adopt the S-matrix point of view in which the interference between overlapping levels of the same J^π is accounted for properly in Eq. (5) with the understanding that the sum of the partial widths for each resonance now exceeds its total width.[28]]

We applied Eq. (5) in several energy regions of the α_0 and α_1 excitation functions and extracted parameters for a total of 25 levels in ^{20}Ne. The results are summarized in Table II for elastic scattering resonances and Table III for inelastic scattering resonances. (Numerical values for the quantity Γ_{α_i}/Γ reported in Ref. 5 are too large by 11.8%.) The center of mass widths listed in the tables have already had our estimated experimental energy resolution unfolded. Two effects arise when the experimental energy broadening is comparable to the natural width of an observed level. One effect is, of course, an in-

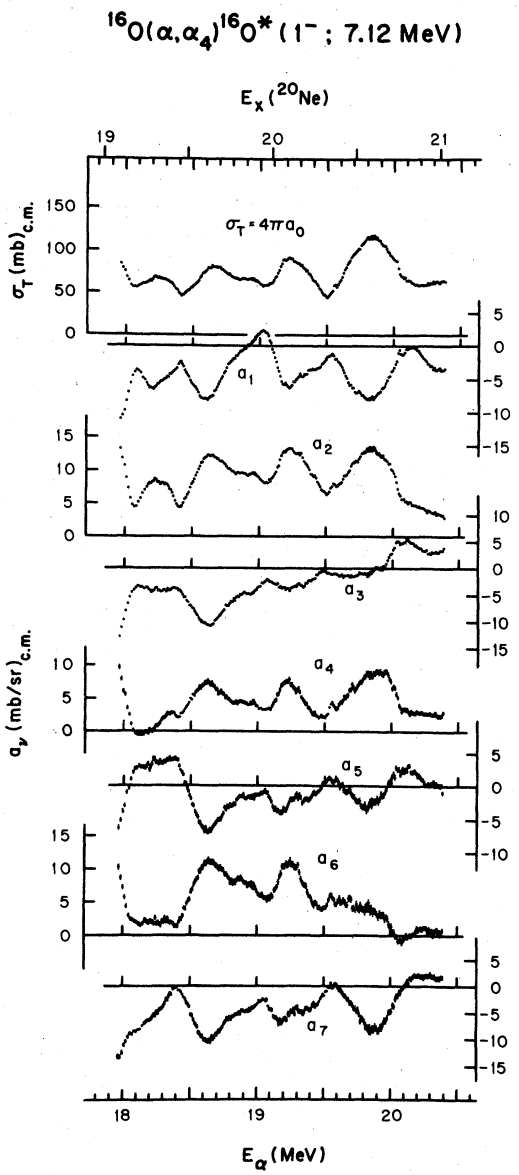

FIG. 21. Lower order coefficients of the Legendre polynomial expansion as a function of bombarding energy for the reaction $^{16}O(\alpha, \alpha_4)^{16}O$.

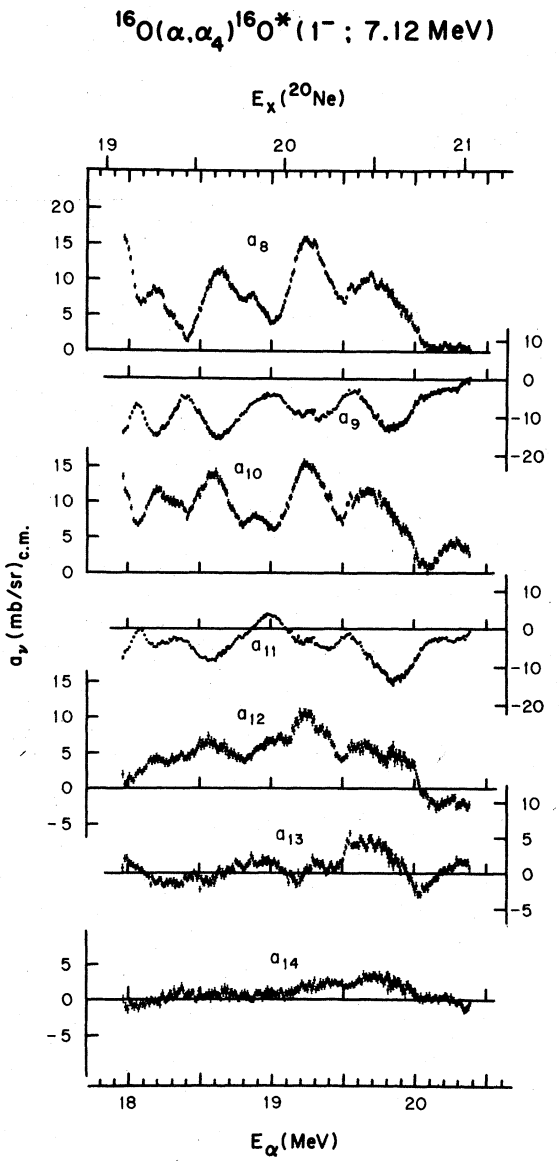

FIG. 22. Higher order Legendre coefficients for the reaction $^{16}O(\alpha, \alpha_4)^{16}O$.

crease in the observed total width of the level. We assumed that the experimental widths were the quadrature sum of the natural resonant width and the experimental broadening. The other effect concerns the branching ratio Γ_{α_i}/Γ. When experimental broadening smears a resonance's interference pattern the pattern's amplitude is always reduced. In the case of only a single open channel (say elastic scattering with $\Gamma_{\alpha_0} \equiv \Gamma$) neither Eq. (3) nor Eq. (5) will reproduce the data unless the experimental broadening is accounted for. For example, Steck[15] corrects for the effect explicitly by averaging the fitting function over an energy interval equal to his experimental resolution. For more than one open channel one includes the branching ratio Γ_{α_i}/Γ as an adjustable parameter. While the fitting program will now reproduce both the amplitude and the shape of the interference pattern it will necessarily underestimate the true branching ratio when there is appreciable experimental energy broadening. We assume that the underestimate is by the factor $\Gamma_{exp}/\Gamma_{nat}$, where Γ_{exp} is the experimental width and Γ_{nat} is the natural width. The branching

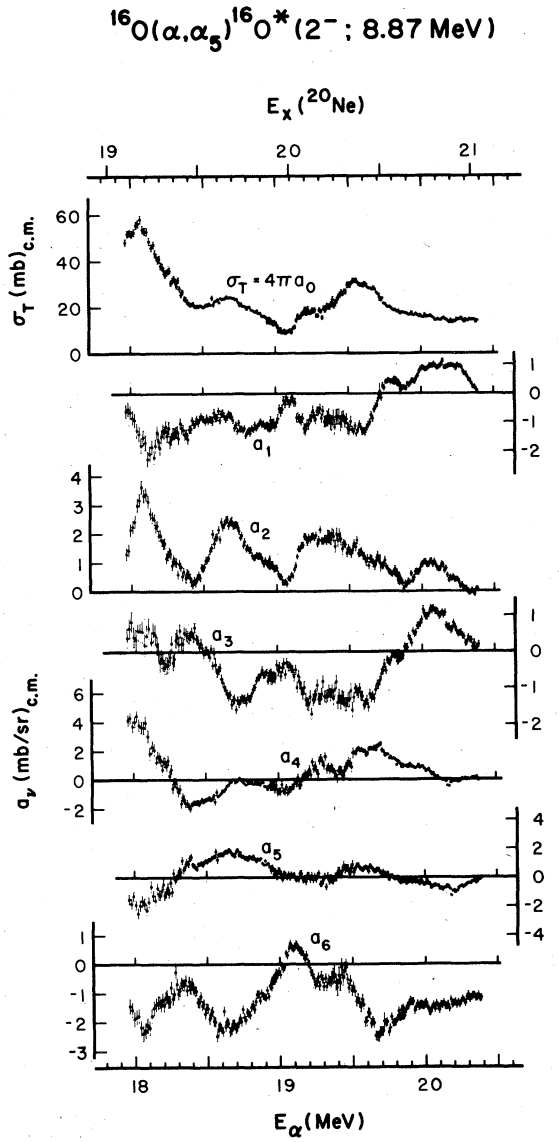

FIG. 23. Lower order coefficients of the Legendre polynomial expansion as a function of bombarding energy for the reaction $^{16}O(\alpha,\alpha_5)^{16}O$.

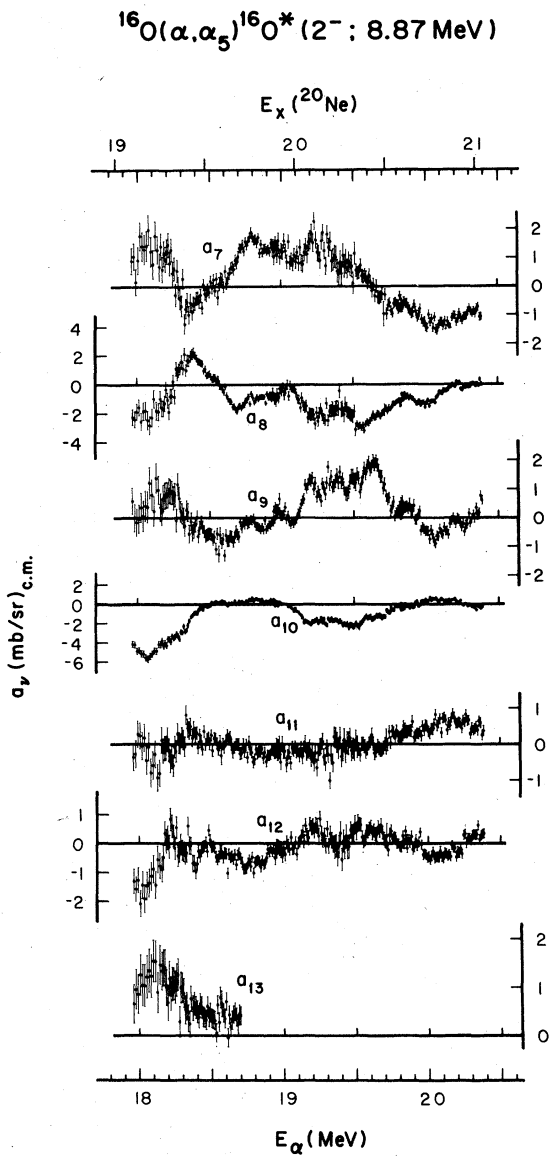

FIG. 24. Higher order Legendre coefficients for the reaction $^{16}O(\alpha,\alpha_5)^{16}O$.

ratios in Tables II and III have been corrected for this effect. For all of the resonances with E_α < 18 MeV the energy resolution is about 15 keV, most of which (~13 keV) arises from energy straggling of the incident α beam in the target gas. For E_α > 18 MeV the experimental resolution was approximately 8 keV.

The uncertainties in the resonant parameters reported in Tables II and III were estimated by varying each resonant parameter separately until the χ^2 (evaluated within $\pm 2\Gamma$ of the resonant energy E_r) doubled. The change in each parameter that doubled χ^2 is our estimate of that parameter's uncertainty. Unfortunately, we did not analyze any of the resonances in both of the reaction channels α_0 and α_1. All but one of the α_0 resonances in Table II are from our DS-1 for which we have no α_1 data. The elastic scattering resonance at $E_\alpha = 19.953$ MeV that occurs in a region where we also have α_1 data does not appear in the α_1 channel (see the discussion of this level below). Most of our analysis of elastic scattering was of the relatively narrow levels (usually with $\Gamma_{c.m.} \leq 100$ keV). We found it much easier to exploit the newly developed fitting procedure in energy regions having only a few rather sharp features,

and thus some gaps remain between the regions we analyzed. With additional effort one might extract many more level parameters from the α_0 data and I plan to attempt this in the future. In the following subsections I discuss the fitted energy regions in order of increasing energy.

A. Energy region from E_α = 14.65 to 15.04 MeV

Häusser *et al.*[3] at Chalk River reported three ^{20}Ne levels in this energy region (see Table II). While we could easily remove the ambiguity encountered by Häusser *et al.* as to a 2^+, 4^+, or 6^+ assignment for the $E_\alpha = 14.721$-MeV level (it has $J^\pi = 6^+$), we could not fit the energy region near $E_\alpha = 14.93$ MeV with their suggested 0^+ or 2^+ level assignments. To obtain satisfactory results five levels between $E_\alpha = 14.65$ and 15.04 MeV were required. Our best fit to this region, shown in Fig. 25, includes a $J^\pi = 5^-$ level at $E_\alpha = 14.980$ MeV for which the Chalk River group suggested 1^-, 3^-, or 7^-. Assignment of spin for this level was made difficult by its very low strength in the elastic channel. (Note that $\Gamma_{\alpha_0}/\Gamma = 0.06$. The state appears much more strongly in the α_{1+2} and the α_3 excitation functions. See Figs. 5 through 8.) While our analysis definitely excluded assignments of 1^- or 7^- for this level, and we prefer $J^\pi = 5^-$, the 3^- assignment is almost as likely. The evidence for our other four spin assignments in this region is quite strong. Other choices of J^π for these states typically doubled the χ^2/degree of freedom of the best fit. We also note that our width of 79 keV for the 4^+ state is 31 keV lower than the width of the 0^+, 2^+ level of Häusser *et al.* We speculate that this may be the result of their fitting the region with too few levels. We observed such an effect in our work. Without the 3^- level at $E_\alpha = 14.886$ MeV, for example, our fitting program tended to increase the width of any state we tried at $E_\alpha = 14.93$ MeV.

Hindi *et al.*[16] have recently reported the observation of a $J^\pi = 7^-$ state at $E_x = 16.581 \pm 0.010$ MeV via the reaction $^{12}C(^{12}C,\alpha)^{20}Ne^*(\alpha_0)^{16}O$. This resonant energy is in good agreement with our $E_x = 16.577 \pm 0.012$ MeV (see Table II), but the width of 150 ± 30 keV of Hindi *et al.* is nearly double our 86 ± 6 keV.

Sanders *et al.*[17] also reported a $J^\pi = 7^-$ state in this energy region that they observed via $^{16}O(^{12}C, ^8Be)^{20}Ne^*(\alpha_0)^{16}O$. However, their resonant energy of $E_x = 16.63$ MeV exceeds ours by ~50 keV, and they claim a width of 190 ± 40 keV and a branching ratio Γ_{α_0}/Γ of 0.90 ± 0.10. The $J^\pi = 7^-$ state that we see at $E_x = 16.577$ MeV has a much smaller width (86 keV) and a branching ratio of only 45%. A single $J^\pi = 7^-$ state with $\Gamma_{\alpha_0}/\Gamma = 0.9$ as reported in Ref. 17 should produce very large effects in our $^{16}O(\alpha, \alpha_0)^{16}O$ excitation functions and so would be hard to miss. However, a broad resonance near the edge of our fitting region can be lumped into the background term. This is unlikely for the parameters quoted in Ref. 17.

B. Energy region from E_α = 15.08 to 15.22 MeV

The only prominent feature in this region (see

TABLE II. ^{20}Ne levels observed via $^{16}O(\alpha,\alpha_0)^{16}O$.

					Previous $^{16}O(\alpha,\alpha_0)^{16}O$ work[a]			
E_α (MeV ± keV)	E_x (MeV ± keV)	$\Gamma_{c.m.}$ (keV ± keV)	$\frac{\Gamma_{\alpha_0}}{\Gamma}$	J^π	E_x (MeV)	$\Gamma_{c.m.}$ (keV)	J^π	Ref.
14.721 ± 15	16.502 ± 12	25 ± 3	0.473 ± 0.024	6^+	16.509	23	2^+, 4^+, 6^+	3
14.815 ± 15	16.577 ± 12	86 ± 6	0.446 ± 0.019	7^-				
14.886 ± 17	16.634 ± 14	51 ± 14	0.173 ± 0.014	3^-				
14.928 ± 16	16.667 ± 13	79 ± 11	0.259 ± 0.025	4^+	16.672	110	0^+, 2^+	3
14.980 ± 18	16.709 ± 14	14 ± 7	0.062 ± 0.026	$5^-(3^-)$	16.718	10	1^-, 3^-, 7^-	3
15.150 ± 15	16.846 ± 12	16 ± 5	0.126 ± 0.021	5^-	16.853	10	5^-	3
15.532 ± 15	17.150 ± 12	33 ± 3	0.291 ± 0.019	5^-	17.161	37	$5^-(7^-)$	3
15.601 ± 15	17.205 ± 12	142 ± 9	0.460 ± 0.019	4^+				
15.687 ± 16	17.274 ± 13	52 ± 10	0.155 ± 0.019	4^+	17.279	32	1^-, 3^-, 4^+	3
15.721 ± 17	17.301 ± 14	213 ± 12	0.237 ± 0.013	8^+	17.3	60		1
15.837 ± 17	17.394 ± 14	241 ± 13	0.209 ± 0.012	$9^{(+)}$				
16.625 ± 10	18.024 ± 8	35 ± 3	0.372 ± 0.018	5^-	18.021	45	2^+, 5^-, 6^+	3
16.746 ± 10	18.120 ± 8	29 ± 3	0.420 ± 0.024	7^-	18.112	33	7^-	3
19.953 ± 11	20.683 ± 9	75 ± 9	0.247 ± 0.018	9^-	20.70	120	9^-	2

[a] See the discussion in the text for previous observations of these levels via other reaction channels.

TABLE III. ^{20}Ne levels observed via $^{16}O(\alpha,\alpha_1)^{16}O$.

E_α (MeV ± keV)	E_x (MeV ± keV)	$\Gamma_{c.m.}$ (keV ± keV)	$\frac{(\Gamma_{\alpha_0}\Gamma_{\alpha_1})^{1/2}}{\Gamma}$	J^π
17.988 ± 12	19.113 ± 10	149 ± 18	0.420 ± 0.012	6^+
18.250 ± 11	19.322 ± 9	123 ± 10	0.272 ± 0.014	6^+
18.393 ± 12	19.437 ± 10	102 ± 7	0.466 ± 0.012	6^+
18.568 ± 13	19.577 ± 11	50 ± 8	0.196 ± 0.027	7^-
18.658 ± 12	19.648 ± 10	89 ± 8	0.332 ± 0.012	6^+
18.990 ± 15	19.914 ± 12	203 ± 19	0.379 ± 0.017	5^-
19.261 ± 21	20.130 ± 17	156 ± 21	0.301 ± 0.020	7^-
19.495 ± 15	20.317 ± 12	203 ± 19	0.343 ± 0.021	7^-
19.640 ± 20	20.433 ± 16	346 ± 32	0.444 ± 0.020	6^+
20.076 ± 14	20.782 ± 11	122 ± 13	0.395 ± 0.020	7^-
20.249 ± 15	20.920 ± 12	181 ± 22	0.339 ± 0.017	7^-

Figs. 3 and 4) is a $J^\pi = 5^-$ level at $E_\alpha = 15.150$ MeV which had been previously assigned by Ref. 3. We confirm their assignment. Figure 26 illustrates at all 16 angles our best fit to this resonance and at a few angles samples of the best fit if other l values are assumed. For an incorrect choice of the resonant l the fit was always unable to reproduce the resonant behavior at several of

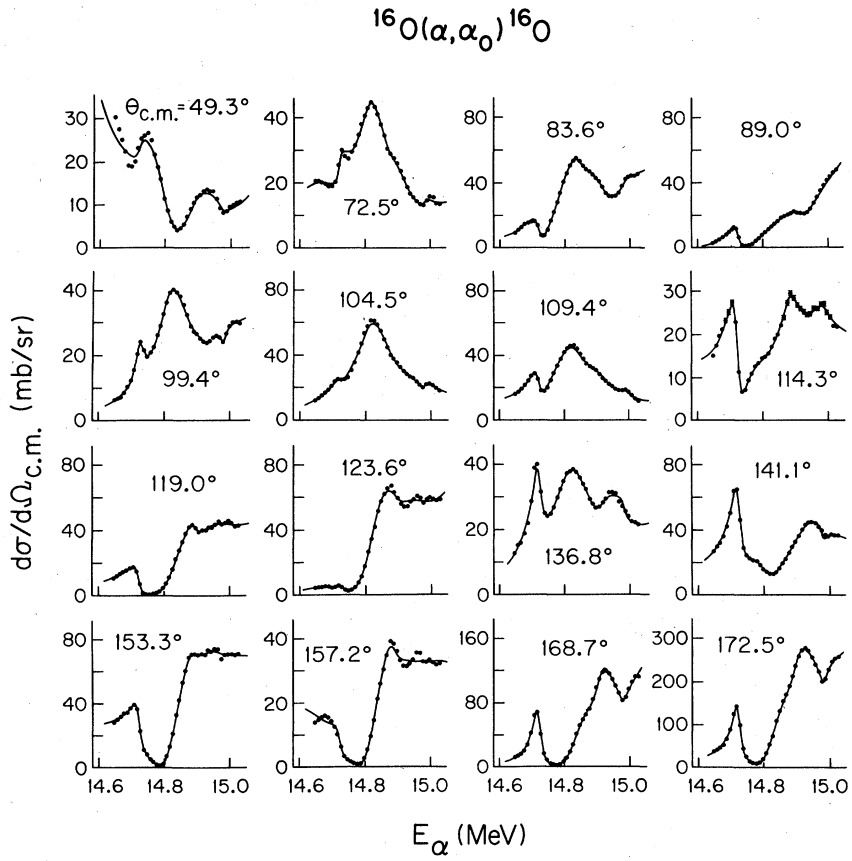

FIG. 25. Fit to the elastic scattering excitation functions in the bombarding energy range 14.65 to 15.04 MeV. The fit shown here included five resonances at (J^π, Γ_{α_0}/Γ, $\Gamma_{c.m.}$ in parentheses) $E_\alpha = 14.721$ MeV (6^+, 0.473, 25 keV); 14.815 MeV (7^-, 0.446, 86 keV); 14.886 MeV (3^-, 0.173, 51 keV); 14.928 MeV (4^+, 0.259, 79 keV); and 14.980 MeV (5^-, 0.062, 14 keV). The overall χ^2/degree of freedom was 2.77 with the largest contribution from the $\theta_{c.m.} = 49.3°$ data.

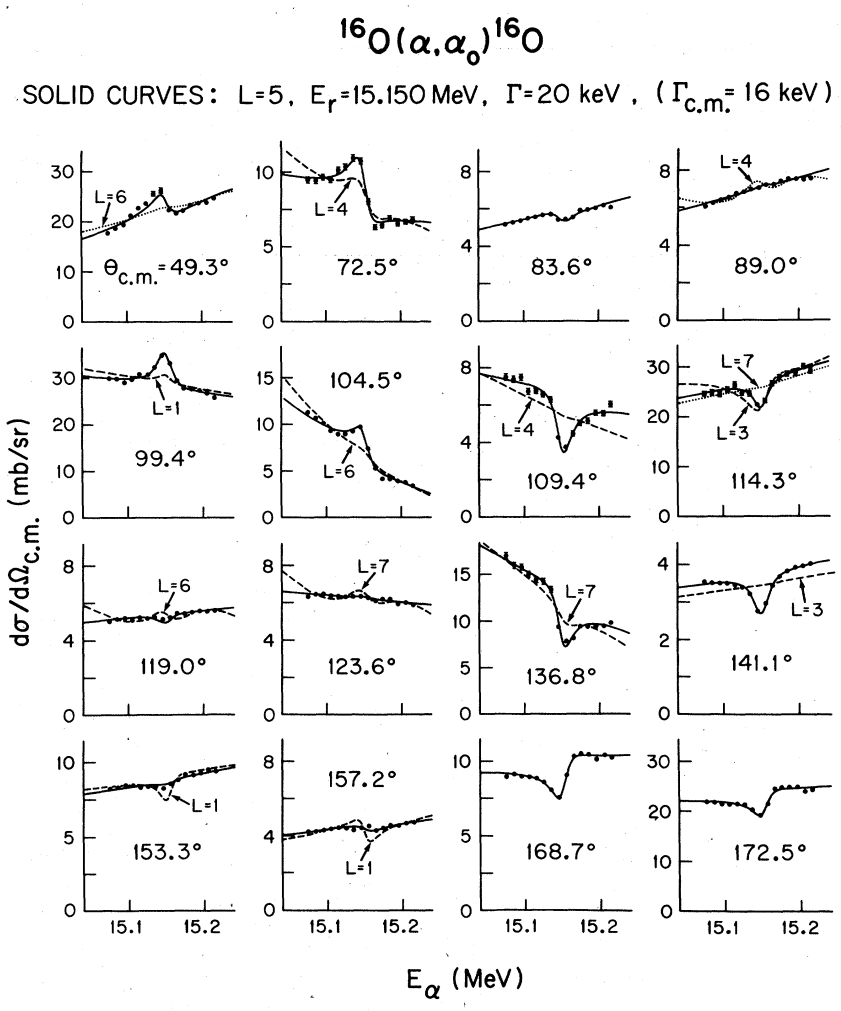

FIG. 26. Elastic scattering resonance at E_α=15.150 MeV. The overall χ^2/degree of freedom for the solid curves (l=5) was 0.88. The dotted and dashed curves are samples of the best fit at some angles if other resonant l values are assumed. For all other choices of l between 0 and 7 the χ^2/d.f. exceeded 2.2.

the angles. As expected the disagreement was most pronounced when the data exhibited large structure at angles for which the Legendre polynomial for the assumed l value was nearly zero.

C. Energy region from E_α = 15.48 to 15.96 MeV

The Chalk River group[3] reported two narrow resonances in this energy region: one at E_α = 15.547 MeV for which they preferred a 5$^-$ assignment (but could not exclude 7$^-$) and another at E_α = 15.695 MeV with J^π of either 1$^-$, 3$^-$, or 4$^+$. We observed a similar structure in our excitation functions, but we also saw evidence for another broader level between the two narrower states (see Figs. 3 and 4, especially $\theta_{c.m.}$ = 49.3° and angles backward of 130°). Samples for eight out of sixteen angles of the best fit to the excitation functions (for $E_\alpha \leq 15.75$ MeV) are shown in Fig. 27. We initially estimated ~32 keV (the value reported by Häusser *et al.*) for the width of the level at E_α = 15.687 MeV, but the fitting program always increased the width to ~52 keV, reducing χ^2 by as much as a factor of 2. Mehta, Hunt, and Davis[1] reported a level of width 60 keV (no spin assignment) at essentially the same energy. Similar resonant structure in this energy region also appears in the α_{1+2}, α_3, and α_4 excitation functions (see Figs. 5 through 10). The J^π=5$^-$ level at E_α = 15.532 MeV is especially pronounced in the α_{1+2} and α_4 data.

Several authors have reported a high spin state near 17.27 MeV excitation in ^{20}Ne (corresponding to E_α = 15.68 MeV). Fifield *et al.*,[18] studying

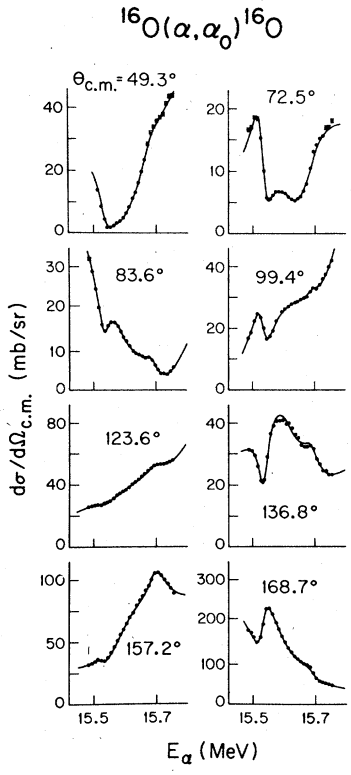

FIG. 27. Eight sample fits (out of a total of sixteen) to elastic scattering data in the bombarding energy range 15.48 to 15.75 MeV. The fit included three ^{20}Ne levels at (J^π, Γ_{α_0}/Γ, $\Gamma_{c.m.}$ in parentheses) $E_\alpha = 15.532$ MeV (5^-, 0.291, 33 keV); 15.601 MeV (4^+, 0.460, 142 keV); and 15.687 MeV (4^+, 0.155, 52 keV). Overall χ^2/d.f. was 1.17.

triple angular correlation of the two alpha particles and the γ ray from the reaction $^{12}C(^{12}C, \alpha)^{20}Ne^*(\alpha)^{16}O^*(\gamma)$ assigned a spin of 9^- to a state at 17.40 ± 0.02 MeV. Artemov *et al.*[19] also observed a 9^- state at 17.35 ± 0.10 MeV via the $^{16}O(^6Li, d)^{20}Ne^*(\alpha)^{16}O$ angular correlation experiment. Artemov *et al.* point out, however, that these may not be the same ^{20}Ne level since the state formed via (^{12}C, α) decays with 99% probability to the 6.13-MeV excited state of ^{16}O while the state they observed via (^{6}Li, d) decays with 40% probability to the ^{16}O ground state. The Soviet group reported a width of 35 ± 15 keV for the $E_x(^{20}Ne) = 17.35$-MeV 9^- state. Cobern *et al.*[20] also observed strong alpha particle transfer via $^{16}O(^7Li, t)^{20}Ne$ to a state at 17.27 ± 0.02-MeV excitation, but they did not assign a spin or width to the level. However, Sanders *et al.*[17] report an 8^+ assignment for a 17.30-MeV state with $\Gamma = 220 \pm 40$ keV and $\Gamma_{\alpha_0}/\Gamma = 0.40 \pm 0.10$. We were unable to fit the $E_\alpha = 15.687$-MeV ($E_x = 17.273$ MeV) level with either 8^+ or 9^- resonant spins. However, very recently upon expanding the fitted region to $E_\alpha = 15.96$ MeV and including both an 8^+ and a 9^- state, a satisfactory fit resulted (χ^2/d.f. = 1.07). Our resonant energy ($E_x = 17.301$ MeV) and $\Gamma = 213$ keV for the 8^+ level agrees with Sanders *et al.*[17] but our $\Gamma_{\alpha_0}/\Gamma = 0.24$ is less than their 0.40 ± 0.10. The necessity for both an 8^+ and a 9^- level in the fitted region removes the discrepancy between the angular correlation data of Ref. 17 and of Ref. 19 since their different reactions may emphasize different states. Some overlap of the two states probably accounts for the poor fits of both sets of angular correlation data. [We ignore the anomalously small width ($\Gamma = 35 \pm 15$ keV) of Artemov *et al.*[19] because it arises indirectly from the cross section and kinematics of an assumed direct reaction.]

D. Energy region from E_α = 16.60 to 16.80 MeV

Häusser *et al.*[3] reported three levels in this region: a very narrow 7^- level at $E_\alpha = 16.598$ MeV ($E_x = 18.001$ MeV, $\Gamma_{c.m.} < 10$ keV), a level at 16.623 MeV ($E_x = 18.021$ MeV) with J^π of either 2^+, 5^-, or 6^+ ($\Gamma_{c.m.} = 45$ keV), and a 7^- level at $E_\alpha = 16.737$ MeV ($E_x = 18.112$ MeV, $\Gamma_{c.m.} = 33$ keV). A 7^- level at excitation energy 18.12 MeV in ^{20}Ne has also been observed in other reactions: Panagiotou *et al.*[21] used the $^{12}C(^{12}C, \alpha)^{20}Ne^*(\alpha)^{16}O$ reaction and assigned $J^\pi = 7^-$ on the basis of their angular correlation studies. Medsker *et al.*[22] also reported a state at 18.11-MeV excitation populated by the $^{12}C(^{12}C, \alpha)^{20}Ne$ reaction, but they did not make a spin assignment. Young *et al.*[23] assigned $J^\pi = 7^-$ based on their angular correlation work on the same reaction as Ref. 21. We observed the two larger-width states in our excitation functions (see Figs. 3 and 4). Both of these resonances also appear in our α_{1+2} and α_3 data (see Figs. 5 through 8) but the 7^- level is nearly absent from our α_4 excitation function (see Figs. 9 and 10). We did not resolve the narrow 7^- state (the energy resolution and step size of Häusser *et al.* was 4 keV and 3 keV, respectively, compared to our 15 keV and 10 keV). Since the state at $E_\alpha = 16.62$ MeV showed pronounced structure at center of mass angles 49.3°, 104.5°, and 157.2° which are all near zeroes of the P_6 Legendre polynomial, we easily excluded the possible 6^+ spin-parity of Ref. 3. Figure 28 illustrates sample fits at several angles with a 7^- level at $E_\alpha = 16.625$ MeV. The 5^-, 7^- combination clearly resulted in a much better description of the data.

E. Energy region from E_α = 18.0 to 20.4 MeV

In the region of excitation energy from $E_x = 19.1$ to 21.0 MeV (corresponding to $E_\alpha = 18.0$ to 20.4 MeV) at least ten ^{20}Ne levels have been identified

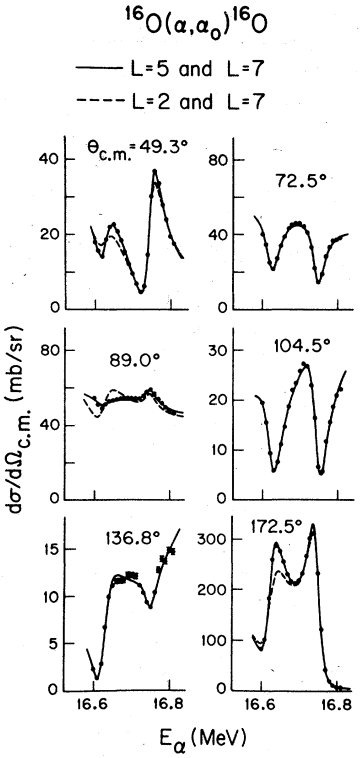

FIG. 28. Six sample fits to elastic scattering data in the bombarding energy range 16.60 to 16.80 MeV. The solid curves represent the best fit (χ^2/d.f.=2.35) to this energy region and correspond to two resonances at (J^π, Γ_{α_0}/Γ, $\Gamma_{c.m.}$ in parentheses) E_α=16.625 MeV (5$^-$, 0.372, 35 keV) and 16.746 MeV (7$^-$, 0.420, 29 keV). The dashed curves at three of the angles are samples of the best fit (χ^2/d.f.=13.5) if $J^\pi=2^+$ is assumed (instead of 5$^-$) for the level at E_α=16.625 MeV.

previously.[24] MHD[1] observed in their $^{16}O(\alpha,\alpha_0)^{16}O$ excitation curves three broad resonant structures listed in Ref. 24 at excitation energies of 19.16, 19.40, and 19.84 MeV. They assigned $J^\pi=6^+$ to all three levels by inspection of their 8-point angular distributions. The only other elastic alpha scattering work in this energy region was that of BH[2] who assigned J^π values of 7$^-$, 6$^+$, 7$^-$, 9$^-$, and 7$^-$ to states at E_x=20.0, 20.4, 20.4, 20.67, and 21.08 MeV, respectively. Except for the 9$^-$ level, all of the MHD and BH states have resonant energies that are uncertain by at least 100 keV, and have center of mass widths in the range 200 to 360 keV. The E_x=19.16-MeV level of MHD has also been observed by Belote *et al.*[25] via the $^{12}C(^{14}N,{}^6Li)^{20}Ne$ reaction. A few levels in this region have been reported in the $^{16}O(^6Li,d)^{20}Ne$ and $^{16}O(^7Li,t)^{20}Ne$ alpha transfer reactions. Artemov *et al.*[26,27] claim two $J^\pi=7^-$ states at excitation energies 19.4±0.1 and 19.9±0.1 MeV, both with $\Gamma_{c.m.}$=400 keV, and another[27] at 20.8±0.1 MeV (no width reported) with $J^\pi=7^-(6^+)$. In view of the large uncertainties in both the energies of Artemov *et al.* and the BH resonant energies, the state at E_x=19.9 MeV of Artemov *et al.* may be the same 7$^-$ level observed by BH at E_x=20.15 MeV and it is so listed in Ref. 24 with E_x=20.0±0.1 MeV and $\Gamma_{c.m.}$=300 keV. Cobern *et al.*[20] observed via the $^{16}O(^7Li,t)^{20}Ne$ reaction two states at E_x=20.58±0.04 and 21.00±0.025 MeV (apparently subsequently changed in Ref. 24 to 20.67 and 21.08 MeV, respectively), but did not assign their spin-parities. Reference 24 now identifies the E_x=20.67 and 21.08-MeV levels of Cobern *et al.* with the two $J^\pi=9^-$ states seen as $^{16}O(\alpha,\alpha_0)^{16}O$ resonances by BH at 20.70 and 21.10 MeV.

We see eleven ^{20}Ne levels (see Table III) in this energy range which decay by α_1 emission: one has $J^\pi=5^-$, five have $J^\pi=6^+$, and five have $J^\pi=7^-$. The $J^\pi=9^-$ state at E_x=20.683 MeV (E_α=19.953 MeV) is present in the α_0, α_2, and α_3 channels (but absent from α_1, α_4, and α_5). The appearance of the 9$^-$ level in only the α_0, α_2, and α_3 cross sections may arise in part from the difference in the angular momentum barrier between these and

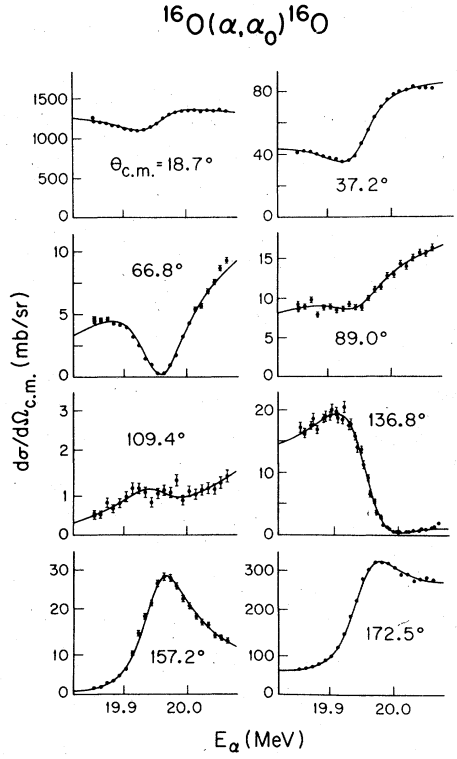

FIG. 29. Eight sample fits to the elastic scattering resonance at E_α=19.953 MeV. The level has J^π=9$^-$, $\Gamma_{c.m.}$=75 keV, and ratio of elastic to total width Γ_{α_0}/Γ=0.247. Overall χ^2/d.f.=1.37.

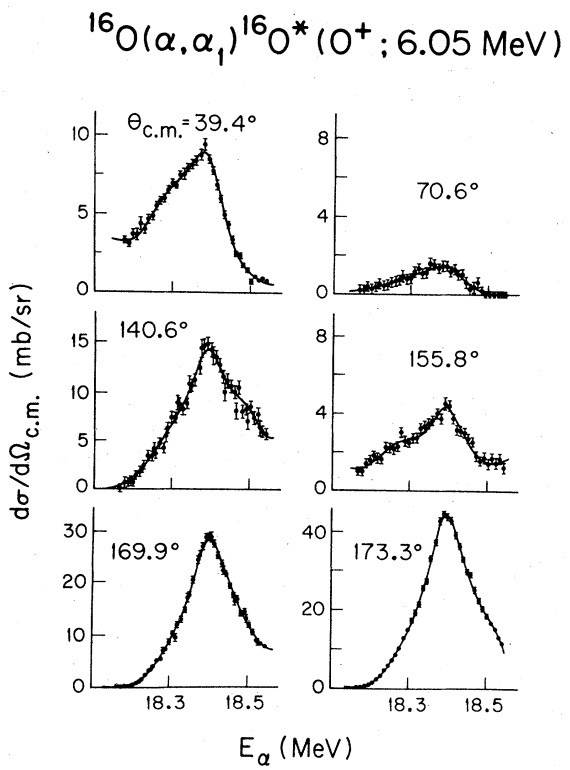

FIG. 30. Six sample fits to inelastic scattering (α_1) data in the bombarding energy range 18.17 to 18.54 MeV. The fit corresponds to three ^{20}Ne levels at [J^π, $(\Gamma_{\alpha_0}\Gamma_{\alpha_1})^{1/2}/\Gamma$, $\Gamma_{c.m.}$ in parentheses] E_α=18.250 MeV (6^+, 0.272, 123 keV); 18.393 MeV (6^+, 0.466, 102 keV); and 18.568 MeV (7^-, 0.196, 50 keV). Overall χ^2/d.f. which included data at 20 angles and 50 energies was 0.86.

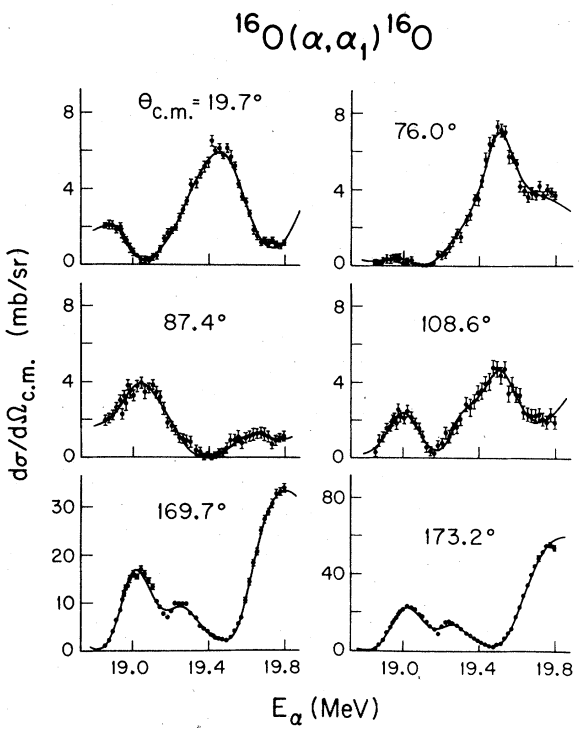

FIG. 31. Sample fits to inelastic scattering (α_1) data in the bombarding energy range 18.80 to 19.80 MeV. To fit this 1-MeV wide energy region we used data at every other energy in our $^{16}O(\alpha,\alpha_1)^{16}O$ excitation functions. The fit (χ^2/d.f.=1.28) required four ^{20}Ne levels at [J^π, $(\Gamma_{\alpha_0}\Gamma_{\alpha_1})^{1/2}/\Gamma$, $\Gamma_{c.m.}$ in parentheses] E_α=18.99 MeV (5^-, 0.379, 203 keV); 19.261 MeV (7^-, 0.301, 156 keV); 19.495 MeV (7^-, 0.343, 203 keV); and 19.640 MeV (6^+, 0.444, 346 keV).

the other decay channels. The α_1 and α_4 channels with residual nuclei of $I^\pi=0^+$ and 1^- require outgoing orbital angular momenta of $l'=9$ or 8 for decay from a $J^\pi=9^-$ state of ^{20}Ne whereas the α_2 and α_3 channels permit $l'=6$ or 7. Figure 29 illustrates sample fits to elastic scattering data at eight out of a total of 21 angles for the $J^\pi=9^-$ level. The large discrepancy between our width of 75 keV and that of BH (120 keV) is probably traceable to poorer energy resolution in their experiment (50 keV) compared to our 8 keV resolution. Figures 30 and 31 show sample fits to the α_1 excitation functions for a few of the levels that we analyzed. Included in Fig. 30 are two $J^\pi=6^+$ levels at E_α=18.25 and 18.393 MeV (E_x=19.322 and 19.437 MeV) and a 7^- level at E_α=18.568 MeV (E_x=19.577 MeV). With much larger energy steps MHD saw these two 6^+ states as a single 6^+ resonance at E_x=19.4 MeV. The $J^\pi=7^-$ state has not been previously reported. Figure 31 includes four resonances: a 5^- level at E_α=18.99 MeV (E_x=19.91 MeV), two 7^- levels at E_α=19.261 and 19.495 MeV (E_x=20.13 and 20.32 MeV), and a 6^+ level at E_α=19.64 MeV (E_x=20.43 MeV). The $J^\pi=6^+$ state was also observed by BH in elastic scattering, but the other three levels are new assignments. Of the remaining four states in Table III the $J^\pi=6^+$ state at E_α=18.658 MeV is a new assignment. MHD had tentatively assigned $J^\pi=6^+$ to a level at $E_x=19.16\pm0.25$ MeV. We confirm this assignment. Our $J^\pi=7^-$ level at E_α=20.08 MeV (E_x=20.782 MeV) may be the $7^-(6^+)$ state that Artemov *et al.*[26] reported. Besides fixing J^π our $\Gamma_{c.m.}$=122 keV also provides new information for this ^{20}Ne state. Finally, the $J^\pi=7^-$ state that we see at E_α=20.249 MeV (E_x=20.920 MeV) confirms the previous assignments[2,20] of BH and of Cobern *et al.* for such a state at $E_x=21.0\pm0.1$ MeV.

V. CONCLUSIONS

This study of the elastic and inelastic scattering of alpha particles by ^{16}O reports many resonant

structures that decay to the ground or one of the first five excited states of ^{16}O. Our analysis of α_0 resonances confirmed several previous J^π assignments, removed ambiguities in the J^π assignments for five other levels, and resulted in assignments for three levels not previously reported. The spin-parity of one other level is still ambiguous. Several of the ^{20}Ne levels that we see decaying by α_1 emission also confirmed previous assignments. The present work, however, reports the first observation of these states via the $^{16}O(\alpha, \alpha_1)^{16}O$ reaction. For all of the α_1 resonances our analysis provides resonant energies and widths with considerably smaller uncertainties than previously available in the energy range $19.1 \leq E_x \leq 21.0$ MeV. In addition we provide information about the channel strength, namely $(\Gamma_{\alpha_0}\Gamma_{\alpha_1})^{1/2}/\Gamma$. The preponderance of states observed via α_1 with $J = 6$ or 7 suggests that the reaction preferentially excites states with spins corresponding to the so-called grazing angular momentum. For the kinetic energy available in the outgoing channel in the $^{16}O(\alpha, \alpha_1)^{16}O$ reaction a grazing collision corresponds to $l' = 6$ or 7 in the energy range $18.0 \leq E_\alpha \leq 20.4$ MeV. Many other ^{20}Ne states of lower spin and small Γ_{α_1}/Γ probably exist for this energy range. Indeed, there is some evidence for states of even spin and parity that we did not include in the fitting procedure. A qualitative inspection of the data at angles where $P_l(\cos\theta) = 0$ suggests that a weak 4^+ and/or 8^+ level(s) may be present near $E_\alpha = 19$ MeV.[5]

ACKNOWLEDGMENTS

I would like to express my gratitude to Professor H. T. Richards for his continued interest and helpful discussions during all phases of this project. I also thank Professor C. H. Blanchard and Dr. H. V. Smith for their suggestions and sound advice. Data acquisition would have been impossible without the extensive aid of Dr. Rudi Abegg, Dr. D. J. Steck, C. A. Davis, S. R. Riedhauser, L. L. Ames, D. R. Benson, and D. Ercegovic. I am indebted to Dr. A. J. Ferguson of the Chalk River Nuclear Laboratories, Ontario, Canada for his version of the variable metric computer code used in our fitting program. This work was supported in part by the U. S. Department of Energy.

[1]M. K. Mehta, W. E. Hunt, and R. H. Davis, Phys. Rev. 160, 791 (1967).
[2]C. Bergman and R. K. Hobbie, Phys. Rev. C 3, 1729 (1971).
[3]O. Häusser, T. K. Alexander, D. L. Disdier, A. J. Ferguson, A. B. McDonald, and I. S. Towner, Nucl. Phys. A216, 617 (1973).
[4]J. C. Corelli, E. Bleuler, and D. J. Tendam, Phys. Rev. 116, 1184 (1959).
[5]J. H. Billen, Ph.D. thesis, University of Wisconsin, 1978 (unpublished). Available through University Microfilms, Ann Arbor, Michigan.
[6]F. Rose, Ph.D. thesis, University of Wisconsin, 1968 (unpublished). Available through University Microfilms.
[7]D. Pledger, Ph.D. thesis, University of Wisconsin, 1968 (unpublished). Available through University Microfilms.
[8]J. John, J. P. Aldridge, and R. H. Davis, Phys. Rev. 181, 1455 (1969).
[9]See AIP document No. PAPS PRVCA-20-1648-25 for 482 pages of $^{16}O(\alpha, \alpha_i)^{16}O(i = 0, 1, 2, 3, 4, 5)$ differential cross sections and Legendre polynomial coefficients. Order by PAPS number and journal reference from American Institute of Physics, Physics Auxiliary Publication Service, 335 East 45th Street, New York, N. Y. 10017. The price is $7.50 for microfiche or $72.80 for photocopies; airmail additional. Make checks payable to the American Institute of Physics.
[10]B. Carnahan, H. A. Luther, and J. O. Wilkes, *Applied Numerical Methods* (Wiley, New York, 1969).
[11]W. A. Friedman, private communication.
[12]J. M. Blatt and L. C. Biedenharn, Rev. Mod. Phys. 24, 258 (1952).
[13]P. L. Jolivette and H. T. Richards, Phys. Rev. 188, 1660 (1969).
[14]L. McDermott, K. Jones, H. Smotrich, and R. Benenson, Phys. Rev. 118, 175 (1960).
[15]D. J. Steck, Ph.D. thesis, University of Wisconsin, 1976 (unpublished). Available through University Microfilms.
[16]M. Hindi, L. Martz, and P. Parker, Bull. Am. Phys. Soc. 23, 929 (1978).
[17]S. J. Sanders, L. M. Martz, and P. D. Parker, J. Phys. Soc. Japan 44, Suppl. 648 (1978).
[18]L. K. Fifield, R. W. Zurmühle, D. P. Balamuth, and J. W. Noé, Phys. Rev. C 8, 2203 (1973).
[19]K. P. Artemov, V. Z. Gol'dberg, I. P. Petrov, V. P. Rudakov, I. N. Serikov, and V. A. Timofeev, Yad. Fiz. 21, 1157 (1975) [Sov. J. Nucl. Phys. 21, 596 (1976)].
[20]M. E. Cobern, D. J. Pisano, and P. D. Parker, Phys. Rev. C 14, 491 (1976).
[21]A. D. Panagiotou, H. E. Gove, and S. Harar, Phys. Rev. C 5, 1995 (1972).
[22]L. R. Medsker, H. T. Fortune, R. R. Betts, and R. Middleton, Phys. Rev. C 11, 1880 (1975).
[23]K. C. Young, Jr., J. M. Lind, D. P. Balamuth, and R. W. Zurmühle, Bull. Am. Phys. Soc. 22, 527 (1977).
[24]F. Ajzenberg-Selove, Nucl. Phys. A300, 1 (1978).
[25]T. A. Belote, N. Anyas-Weiss, J. A. Becker, J. C. Cornell, P. S. Fisher, P. N. Hudson, A. Menchaca-Rocha, A. D. Panagiotou, and D. K. Scott, Phys. Rev.

Lett. 30, 450 (1973).
[26]K. P. Artemov, V. Z. Gol'dberg, I. P. Petrov, I. N. Serikov, V. P. Rudakov, V. A. Timofeev, R. Wolski, and J. Szmider, Yad. Fiz. 22, 242 (1975) [Sov. J. Nucl. Phys. 22, 125 (1975)].
[27]K. P. Artemov, V. Z. Gol'dberg, I. P. Petrov, V. P. Rudakov, I. N. Serikov, and V. A. Timofeev, Yad. Fiz. 23, 489 (1976) [Sov. J. Nucl. Phys. 23, 257 (1976)].
[28]See K. W. McVoy, Ann. Phys. (N.Y.) 54, 552 (1969).